The Thesis Committee for Logan Marcos Schmidt
Certifies that this is the approved version of the following Thesis:

Monitoring bedrock vadose zone water storage dynamics with time-lapse borehole nuclear magnetic resonance well logging

APPROVED BY
SUPERVISING COMMITTEE:

Daniella Rempe, Supervisor

Ashley Matheny

Zoya Heidari

Monitoring bedrock vadose zone water storage dynamics with time-lapse borehole nuclear magnetic resonance well logging

by

Logan Marcos Schmidt

Thesis

Presented to the Faculty of the Graduate School of

The University of Texas at Austin

in Partial Fulfillment

of the Requirements

for the Degree of

Master of Science in Geological Sciences

The University of Texas at Austin

August 2022

Abstract

Monitoring bedrock vadose zone water storage dynamics with time-lapse borehole nuclear magnetic resonance well logging

Logan Marcos Schmidt, M.S. Geo. Sci.

The University of Texas at Austin, 2022

Supervisor: Daniella Rempe

Bedrock vadose zone water storage dynamics are a critical component of the hydrologic cycle in many catchments, but direct observations of these dynamics are rare. Nuclear magnetic resonance (NMR) methods are sensitive to volumetric water content and to pore chemistry and structure, making NMR a candidate for directly observing bedrock vadose zone water storage dynamics and the material properties associated with them. However, applications of NMR to study water storage in bedrock vadose zones are rare. Here we present the first use of time-lapse borehole nuclear magnetic resonance well logging to monitor and characterize seasonal water content changes in the deeply weathered bedrock vadose zone at two sites in Northern California. The work is presented in two chapters, each of which focuses on one of the two aspects of the NMR measurement: water content and relaxation times. In the first chapter, we evaluate the ability of borehole NMR to quantify water content changes in weathered bedrock. We show strong agreement between estimates of dynamic water storage derived from NMR and independent estimates

from neutron logging and mass balance calculations. The agreement between NMR and neutron estimates of dynamic storage suggests that all seasonally exchanged bedrock water is hosted in fractures, and not the matrix, at these sites. The depths of dynamic storage we observe are up to 9 m and likely reflect the depth extent of root-water uptake. In the second chapter, we document the relationship between bedrock weathering and NMR relaxation times. We find that the sum of echoes (SE) is a useful approach for characterizing NMR relaxation times in the vadose zone, and we use the functional dependence of SE on water content to show that enhanced bedrock weathering extent is associated with faster relaxation times. We find evidence that NMR relaxation times can be sensitive to changes in pore pressure associated with recharge events. The work presented here establishes borehole NMR well logging as a viable method for *in situ* vadose zone monitoring and characterization.

Table of Contents

List of Tables

List of Figures

Acknowledgement of Previous Publication and Contribution Statement

The material contained in “Chapter 1: Quantifying dynamic bedrock vadose zone water storage with time-lapse borehole nuclear magnetic resonance” was published in *Geophysical Research Letters* Volume 47 Issue 22 on 2020-11-28. Logan Schmidt contributed to research design; data collection, management, and analysis; and writing.

Chapter 1: Quantifying dynamic bedrock vadose zone water storage with time-lapse borehole nuclear magnetic resonance

ABSTRACT

Quantifying the volume of water that is stored in the subsurface is critical to studies of water availability to ecosystems, slope stability, and water-rock interactions. In a variety of settings, water is stored in fractured and weathered bedrock as rock moisture. However, few techniques are available to measure rock moisture in unsaturated rock, making direct estimates of water storage dynamics difficult to obtain. Here, we use borehole nuclear magnetic resonance (NMR) at two sites in seasonally dry California to quantify dynamic rock moisture storage. We show strong agreement between NMR estimates of dynamic storage and estimates derived from neutron logging and mass balance techniques. The depths of dynamic storage are up to 9 m and likely reflect the depth extent of root water uptake. To our knowledge, these data are the first to quantify the volume and depths of dynamic water storage in the bedrock vadose zone via borehole NMR.

INTRODUCTION

Water storage in the unsaturated zone is a fundamental component of the hydrologic cycle that regulates evapotranspiration, runoff, and groundwater recharge. Water storage in soils as soil moisture has received considerable attention, and methodology for quantifying dynamic storage in soils exists across scales (Babaeian et al., 2019). However, less attention has been paid to dynamic storage within fractured bedrock, where dynamic water storage can play a critical role in providing water to vegetation

(Schwinning, 2010), dictating the fate of contaminants (Faybishenko et al., 2000; Gwo et al., 2005) and controlling the pace of chemical weathering and biogeochemical cycling (Ireson et al., 2009; Wan et al., 2019). Few techniques are available to document the spatiotemporal patterns of volumetric water content in unsaturated, fractured bedrock environments.

Nuclear magnetic resonance (NMR) is an emerging geophysical method for estimating the water content and hydraulic properties of the unsaturated zone. Geophysical applications of NMR methods, including laboratory, borehole, and surface applications, have become well established over several decades and are routinely used in petroleum engineering (Coates et al., 1999; Dunn et al., 2002) and hydrogeophysics (Behroozmand et al., 2015) to characterize the flow and storage properties of porous media. The NMR measurement is directly sensitive to the hydrogen content of pore fluid and therefore provides robust measurements of volumetric water content. In vadose zone hydrology applications, a distinct advantage of NMR relative to other geophysical methods such as electrical resistivity tomography, seismic, or ground penetrating radar is the ability to directly quantify volumetric water content as well as changes in volumetric water content. Recently, NMR has been employed to estimate water content in the bedrock vadose zone at the field scale via borehole (e.g., Flinchum et al., 2018; Rempe et al., 2018) and surface (e.g., Carrière et al., 2016; Flinchum et al., 2019; Lesparre et al., 2020) deployments. However, borehole NMR has not yet been used monitor the small water content changes that occur in unsaturated weathered bedrock, and it has not yet been established whether such water content changes, and thus dynamic storage, can be reliably quantified with borehole NMR measurements in the complex subsurface environment. Importantly, there is a limit to the fastest decaying signals (shortest relaxation components) that can be captured by borehole NMR instruments, set by the minimum echo spacing of the tool (Behroozmand et al., 2015). This means that water held in the smallest pores and, in the vadose zone, the residual wetting layers with the highest surface/volume ratios may not be included in the NMR estimate of volumetric water content. Such potential petrophysical limitations of NMR for quantifying *in situ* changes in unsaturated water content, including others such as sufficient signal/noise ratio or the presence of minerals with high magnetic susceptibilities (e.g., Keating & Knight, 2008, 2010), have not yet been assessed at the field scale.

Here, we monitor water content changes and quantify dynamic storage associated with fractures in unsaturated bedrock weathering profiles through successive borehole NMR well logging conducted under wet and dry conditions at two seasonally dry field sites. We support our NMR results using the results of neutron moderation logging and hydrologic mass balance techniques and use the agreement among these methods to evaluate borehole NMR as a technique for capturing the magnitude and spatiotemporal patterns of unsaturated dynamic storage in weathered and fractured bedrock.

SITE DESCRIPTION AND METHODS

We exploit two established hillslope study sites—Rivendell and Sagehorn—associated with the Eel River Critical Zone Observatory (ERCZO) in the Northern California Coast Ranges, United States (Figure 1.1). The sites are approximately 20 km apart. The climate is Mediterranean, with warm dry summers and cool wet winters. Mean annual temperature at the site is 13°C and mean annual precipitation (measured from 1981 to 2010) is 1,811 mm (PRISM Climate Group, 2004). The seasonal cumulative precipitation during the 2017 water year was 3,381 mm.

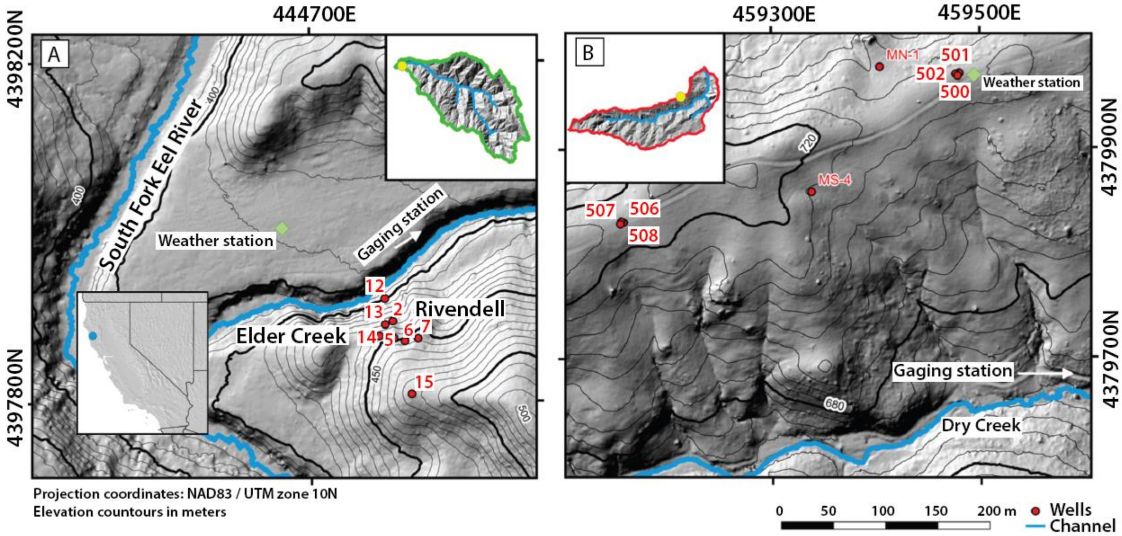

Figure 1.1. Site maps modified from Dralle et al. (2018). Inset shows the state of California with a blue point for the study watersheds location. (a) Bare Earth hillshade map of the Rivendell study area. Inset shows the Elder Creek watershed, and the yellow point corresponds to the Rivendell site. Borehole locations are shown as red points. (b) Bare Earth hillshade map of the Sagehorn study area. Inset shows the Dry Creek watershed, and the yellow point corresponds to the Sagehorn site. Borehole locations are shown as red points

Each study site has a distinct lithologic and ecologic setting. The Rivendell site is underlain by turbidites of the Coastal Belt of the Franciscan Formation, consisting of argillite with sandstone and conglomerate interbeds. The Rivendell boreholes (W7, W12, W13, W14, W15, and W16) are drilled into the deeply weathered argillite and intersect minor sandstone interbeds. The weathering profile—consisting of thin (<1 m thick) soils, up to 4 m of saprolite, and up to 20 m of weathered bedrock—thickens upslope from 4 m near the channel to 25 m at the ridge and shows decreasing fracturing and weathering with depth (Rempe & Dietrich, 2018; Salve et al., 2012). Rivendell hosts a mixed broadleaf/needleleaf evergreen forest. Boreholes W12, W13, W2, W14, W5, W6, W7 and W15 are located on the north-facing slope where Douglas Fir dominate W16 is located on the south-facing slope where madrone and oaks dominate. The Sagehorn site is underlain by the Central Belt of the Franciscan Formation, which is a tectonic mélange that consists of tectonically sheared argillite with coherent blocks of varying sizes composed of different mineralogy. Soils 30–40 cm thick overlie a thin saprolite and unweathered mélange matrix is typically encountered at 2- to 4-m depth (Hahm et al., 2019). W501 is drilled into an argillaceous mélange matrix with herbaceous groundcover, while W503 and W505 are drilled into a sandstone block near a mixture of mature bay and live oaks (Hahm et al., 2018).

Boreholes at both sites were drilled and constructed for downhole moisture monitoring. Holes were drilled without water or drilling fluid via auguring or air-rotary coring (see Table S2 for borehole information). Holes W14, W15, W16, W501, and W503 were drilled with a 3-inch bit and cased snugly with no backfill with 2-inch PVC (outer diameter 2.375 inches), and holes W7, W12, W13, and W505 were drilled with a 4-inch drill bit and cased snugly with no backfill with 3-inch PVC (outer diameter 3.5 inches) (Hahm et al., 2018; Salve et al., 2012). To prevent ponding and preferential flow of infiltrating water down the borehole, well heads were constructed with outward-sloping concrete. Each borehole penetrates the water table and thus encompasses the entire length of the unsaturated zone. We conducted two successive logging campaigns during the summer of 2017. Borehole NMR and neutron well logs were conducted in May (wet conditions, high water table) and August and October (dry conditions and low water table; see Table S1).

Borehole NMR logs were acquired with a Dart NMR Logging System (Vista Clara, Inc., Mukilteo, Washington, USA). Measurements were taken every 0.25 m using the same graduated cable for all well logs. The volume of investigation is a cylindrical shell of height 0.23 m, thickness 1–2 mm, and radius 6.5–7.6 cm, centered on the central axis of the tool (Walsh et al., 2013). The shallowest logged depth is 1.5 m, which is within bedrock and below soils in all boreholes. Each NMR data set was acquired with the Carr-Purcell-Meidboom-Gill pulse sequence at two operational frequencies near 420 and 480 kHz, respectively, with 60 echoes and an echo spacing of 0.5 ms. The data were stacked 168 times, and each stack was separated by a repolarization time (or wait time) of 0.15 s. Before each campaign, the system was calibrated in a shielded water sample in the lab. The NMR data were processed using commercial software (JavelinProcess_v4.4 and JavelinInterpret_v1.8, Vista Clara, Inc.). All stacks, stages, and frequencies associated with each depth interval were combined, and the resulting NMR decay curve was fit with a multiexponential decay function determined via a nonnegative least squares inversion algorithm with second-order Tikhonov regularization using the default software regularization factor of 50. Water content estimated from our NMR measurements, θ_{nmr} (m^3/m^3), was taken as the value of the multi-exponential fit at time equals zero. Noise level was taken as the norm of the residuals after subtracting the multiexponential fit from the data.

Borehole neutron logs were acquired with two neutron gauges: a 501 neutron and gamma probe and a 503-moisture gauge (Instrotek, Concord, CA). Well-log measurements were conducted for 25 s at depth increments of 0.30 m. The starting and ending depth of each survey varied between wells, depending on the height of casing stick up and the depth of the water table at the time of the survey. The volume of investigation is an ill-defined ellipsoid cloud centered on the probe whose size depends strongly on water content. In practice, the measured neutron water content is the mean for a sphere of radius about 15 cm in wet material and 30–70 cm in dry material (Bell, 1987; Gardner, 1986). The linear calibration relation between neutron count, N, and water content, $\theta_{\mathrm{neutron}}$ (m^3/m^3), used for 501 measurements was developed by (Rempe & Dietrich, 2018) using a sand-filled barrel calibration for each borehole diameter. To allow for inter-probe comparison, this calibration was applied to the 501 by converting 501 counts to equivalent 503 count via linear regression of measurements acquired in locations in which water content is invariant (see SI, e.g., Ward et al., 2000; Ward & Wittman, 2009). It is exceptionally challenging to accurately measure absolute θ with a neutron probe (Seyfried et al., 2001; Williams & Sinclair, 1981). This is because depth-by-depth calibrations are not feasible for inaccessible, heterogeneous materials. Without such a calibration, we cannot make accurate measurements of $\theta_{\mathrm{neutron}}$. However, we can achieve much more accurate estimates of water content change $\Delta\theta_{\mathrm{neutron}}$ because it depends only on the slope of the calibration line, and materials differ relatively little in this respect (Bell, 1987). Our study focuses on water content changes; nonetheless, we report the $\theta_{\mathrm{neutron}}$ that results from a constant calibration throughout the profile and consider this to be a "sand-equivalent" water content, i.e., not representative of the water content of the *in situ* material.

To obtain estimates of uncertainty in θ_{nmr} and $\theta_{neutron}$, we performed repeat NMR and neutron measurements at different monitoring locations, using the same methods employed in logging measurements. Uncertainty was estimated as the mean standard deviation of all repeat measurement sets. Uncertainty in changes in water content measured between wet and dry well logs ($\Delta\theta_{nmr}$) is calculated as the square root of the sum of the squared uncertainties in water content (i.e., propagation of error). The uncertainty in depth of the measurement was estimated as 0.5 cm.

Here, each borehole is associated with two sets of water content depth profiles: one derived from successive NMR logs and another derived from successive neutron logs. NMR and neutron logs were acquired within 0–19 days of each other (see Table S3 for the exact logging dates). Based on previous monitoring, we do not expect detectable water content changes greater than the instrument uncertainty of our borehole monitoring tools to occur at the weekly time scale during the dry season at these sites (Hahm et al., 2020; Rempe & Dietrich, 2018). NMR and neutron measurements acquired at the same location at the same time are considered "paired" and allow for intra-method comparison of measurements. For each method, water content change, $\Delta\theta$ (m^3/m^3), is calculated as the difference in θ between wet and dry surveys. Dynamic storage, $S_{dynamic}$ (mm), is calculated as the depth integral of $\Delta\theta$, excluding locations where $\Delta\theta$ is not statistically different from zero (below uncertainty). The depth of dynamic storage is calculated as the depth at which the rate of increasing water content is lower than the rate of increasing uncertainty as $\Delta\theta$ is integrated from the surface. Total storage, S_{total} (mm), is calculated as the depth integral of water content measured in the May NMR well logs, which represent wet conditions. We do not calculate S_{total} from neutron data, because we lack a material-specific, depth-by-depth neutron probe calibration that allows for accurate estimation of $\theta_{neutron}$. To account for differences in the vertical spacing of NMR and neutron measurements (0.3 and 0.25 m, respectively), we linearly interpolated θ_{nmr} and $\Delta\theta_{nmr}$ and resampled the data at 0.25-m intervals.

RESULTS

Water Content Measurement Quality and Uncertainty

We achieved high quality NMR decay curves in unsaturated weathered bedrock. The mean noise level is nearly constant for all NMR measurements at 0.014 m^3/m^3 (standard deviation of 0.005 m^3/m^3). We find no correlation between noise level and θ_{nmr}, measurement location, or measurement date. In nearly all measurements (approximately 94%), signal is larger than noise such that the signal/noise ratio exceeds one. NMR signal amplitudes tend to decay rapidly—an average of eight consecutive echo amplitudes were recorded per measurement before any single amplitude drops below noise level (e.g., Figure 1.2). Of the measurements reported here, 57% include at least five consecutive echo amplitudes above noise level.

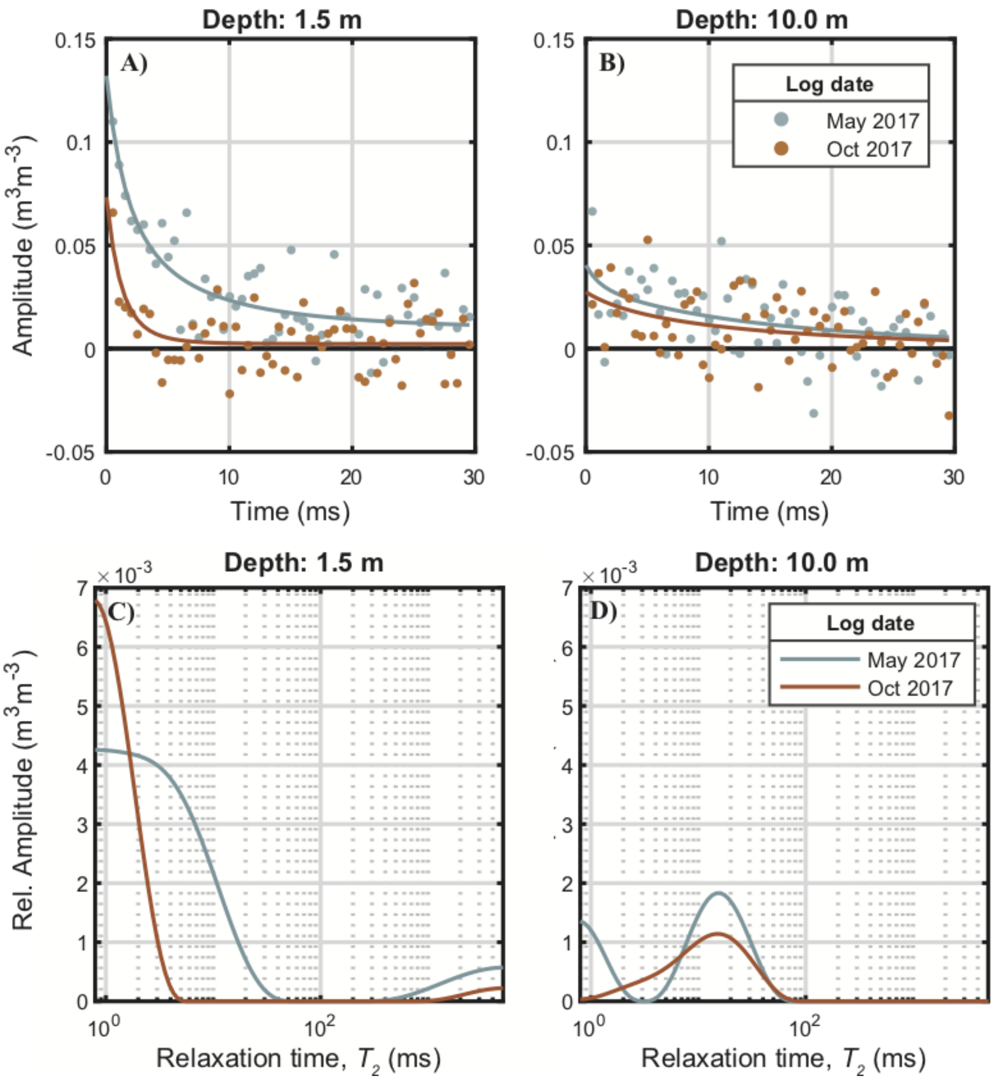

Depth: 1.5 m
Depth: 10.0 m
A)
B)
Log date
May 2017
Oct 2017
Amplitude (m^3m^{-3})
Time (ms)
Depth: 1.5 m
Depth: 10.0 m
C)
D)
Rel. Amplitude (m^3m^{-3})
Relaxation time, T_2 (ms)

Figure 1.2. The effect of drying on the NMR decay-curve (A and B) and relaxation time, T_2, distribution (C and D) is shown for measurements made at 1.5 m depth (A and C) and 10.0 m depth (B and D) in the bedrock vadose zone at Rivendell in W15. Individual NMR decay amplitudes—scaled to units of volumetric water content—are shown as discrete points, and superimposed curves are the multi-exponential fit to these values. The value of the fit at time zero in A and B, and the area under the curve in B and C, is θ_{nmr} for that measurement

Between wet and dry well logs, detectable differences in θ_{nmr} occur above uncertainty (Figures 1.3 and 1.4). Uncertainty in θ_{nmr} is estimated from repeat measurements. The standard deviation of repeat θ_{nmr} ranges from 0.002 to 0.024 m^3/m^3, with a mean of 0.014 m^3/m^3 (the standard deviation of repeat measurements is coincidentally the same as the mean noise level; Figure 1.5). We take this mean as our estimate of θ_{nmr} uncertainty, which is lower than the range of error estimates (0.02–0.10 m^3/m^3) reported by Kass et al. (2017) using the same instrument. Via the propagation of error, the uncertainty in $\Delta\theta_{\mathrm{nmr}}$ is then 0.019 m^3/m^3. Among all monitoring measurements, θ_{nmr} ranges from 0.002 to 0.254 m^3/m^3 with a mean value of 0.078 m^3/m^3. Therefore, nearly all (96%) of θ_{nmr} measurements are larger than uncertainty. Measurements of $\Delta\theta_{\mathrm{nmr}}$ range from −0.060 to 0.108 m^3/m^3 with a mean of 0.016 m^3/m^3. Only 31% of $\Delta\theta_{\mathrm{nmr}}$ measurements are larger than uncertainty, indicating that many of our monitoring locations either do not experience water content changes or experience small changes below detection. Generally, large, detectable differences in θ_{nmr} are concentrated at shallow depths, while at deeper depths, differences tend to be below uncertainty.

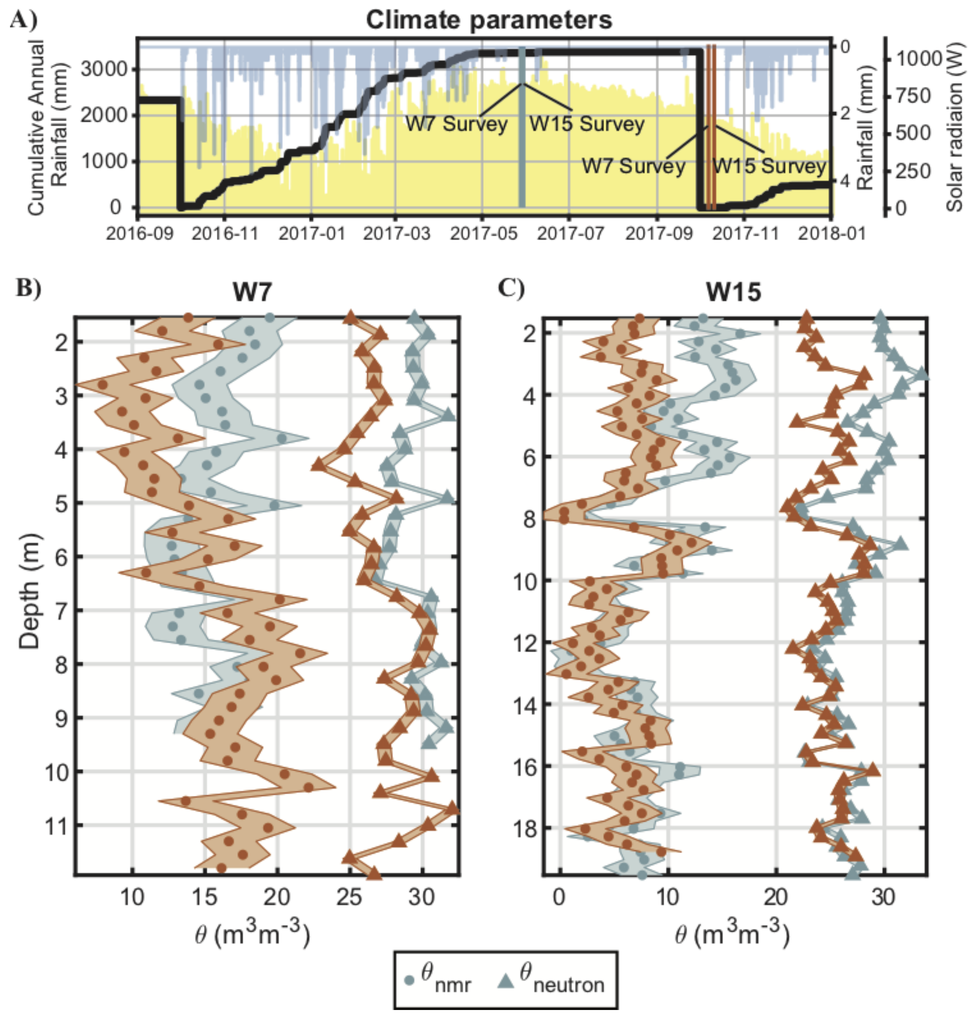

A)
Climate parameters
Cumulative Annual Rainfall (mm)
Rainfall (mm)
Solar radiaion (W)
W7 Survey
W15 Survey
W7 Survey
W15 Survey
2016-09
2016-11
2017-01
2017-03
2017-05
2017-07
2017-09
2017-11
2018-01
B)
W7
C)
W15
Depth (m)
θ (m^{3}m^{-3})
θ (m^{3}m^{-3})
θ_{nmr}
$\theta_{neutron}$

Figure 1.3. Example water content depth profiles which track a seasonal cycle of wetting and drying of a bedrock vadose zone. The timing of water content logs is shown as vertical lines in the (a) time series of rainfall and solar radiation. Successive well logging with NMR (θ_{nmr}) and neutron (θ_{neutron}) tools in (b) W7 and (c) W15 in May (blue) and October (orange) 2017. Note that the absolute magnitude of θ_{neutron} represents a "sand-equivalent" water content and does not accurately represent the in situ water content. Measurements are shown as discrete points, and measurement uncertainty is shown as shaded envelopes. Overlapping envelopes between May and October indicate that change in θ at that depth is below uncertainty. All logging measurements were obtained above the water table at the time of measurement, i.e., the depth extent of measurements is equivalent to the depth extent of the unsaturated zone at the time of measurement.

Like NMR, detectable differences in θ_{neutron} tend to be concentrated at shallow depths, and many monitoring locations did not show changes in water content (Figures 1.3 and 4). Uncertainty in θ_{neutron} is estimated from repeat measurements. The standard deviation of repeat θ_{neutron} ranges from 0.001 to 0.013, with a mean of 0.005 m^3/m^3 (Figure 1.5). We take this mean as our estimate of θ_{neutron} uncertainty. Via the propagation of error, the uncertainty in changes in water content measured between wet and dry well logs ($\Delta\theta$neutron) is then 0.006 m^3/m^3. Among all monitoring measurements, θ_{neutron} ranges from 0.189 to 0.413 m^3/m^3 with a mean value of 0.256 m^3/m^3. All θ_{neutron} values are greater than uncertainty. Change in water content, $\Delta\ \theta_{\text{neutron}}$, ranges from −0.014 to 0.073 m^3/m^3 with a mean of 0.020 m^3/m^3. Of all $\Delta\ \theta_{\text{neutron}}$ values, 87% are greater than uncertainty.

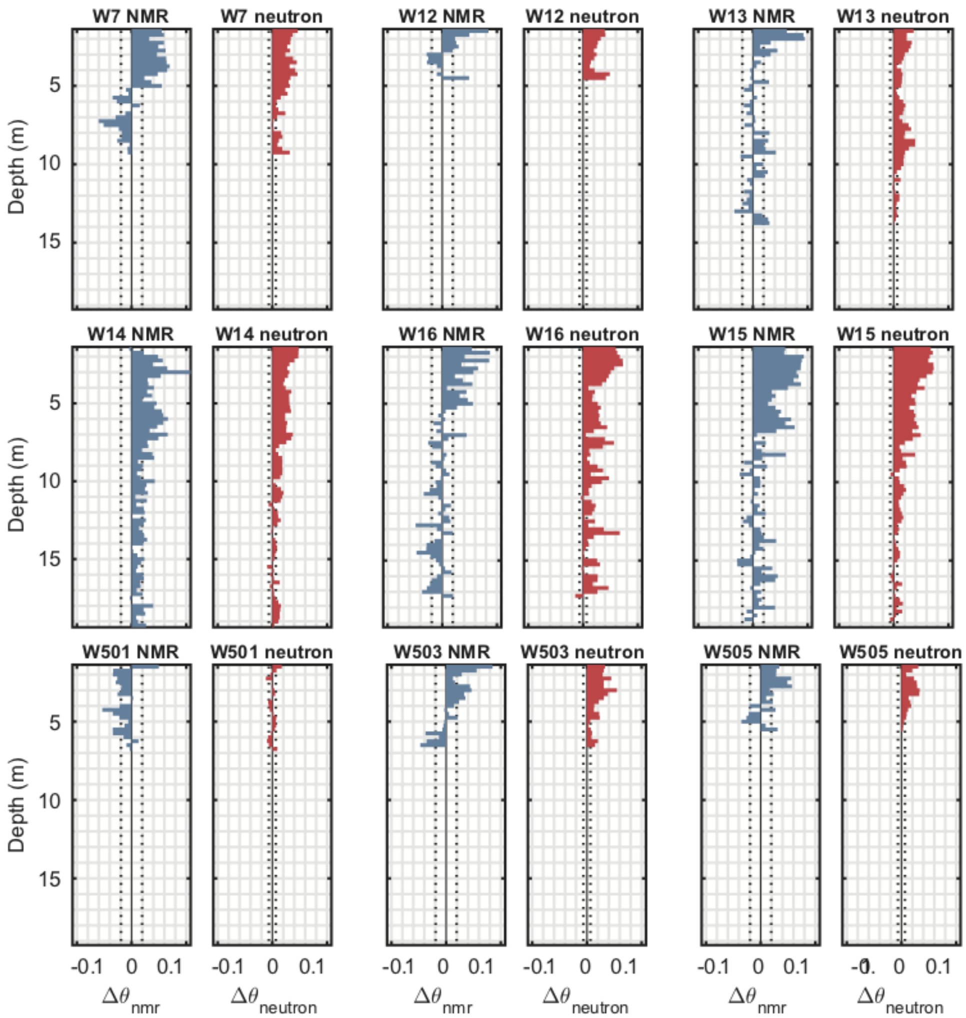
W7 NMR
W7 neutron
W12 NMR
W12 neutron
W13 NMR
W13 neutron
W14 NMR
W14 neutron
W16 NMR
W16 neutron
W15 NMR
W15 neutron
W501 NMR
W501 neutron
W503 NMR
W503 neutron
W505 NMR
W505 neutron
Depth (m)
5
10
15
-0.1 0 0.1
$\Delta\theta_{nmr}$
$\Delta\theta_{neutron}$

Figure 1.4. Water content change depth profiles measured with NMR ($\Delta\theta_{nmr}$) and neutron ($\Delta\theta_{neutron}$) well logs in the unsaturated zone of all study monitoring wells between May and October 2017 (see Table S1 for survey dates). The 68% confidence interval is depicted as vertical dotted lines. $\Delta\theta$ values that lie within this interval are not considered significantly different from zero and are not included in the calculation of dynamic storage. All logging measurements shown were acquired above the depth of the May 2017 water table.

There is agreement in $\Delta\theta$ for both measurement techniques (Figures 1.4 and 1.6). As expected, $\theta_{neutron}$ does not agree with θ_{nmr} (Figures 1.3 and 1.6) due to the sand-pack calibration. However, we note that over the range of water contents measured, this offset is relatively constant and the linear relationship (R2 = 0.52, $p \ll 0.01$) between paired θ_{nmr} and $\theta_{neutron}$ measurements has a slope of nearly one (0.96 ± 0.03) (Figure 1.6).

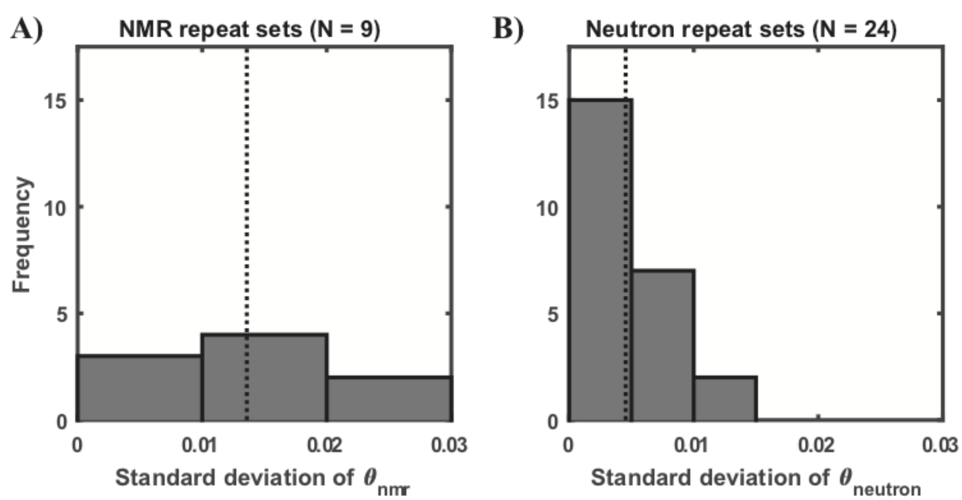

Figure 1.5 The distribution of standard deviation values of water content estimates obtained in repeat measurement sets using NMR (A) and neutron tools (B). In each panel, the dotted black vertical line indicates the mean standard deviation of all repeat sets, which we take as measurement uncertainty.

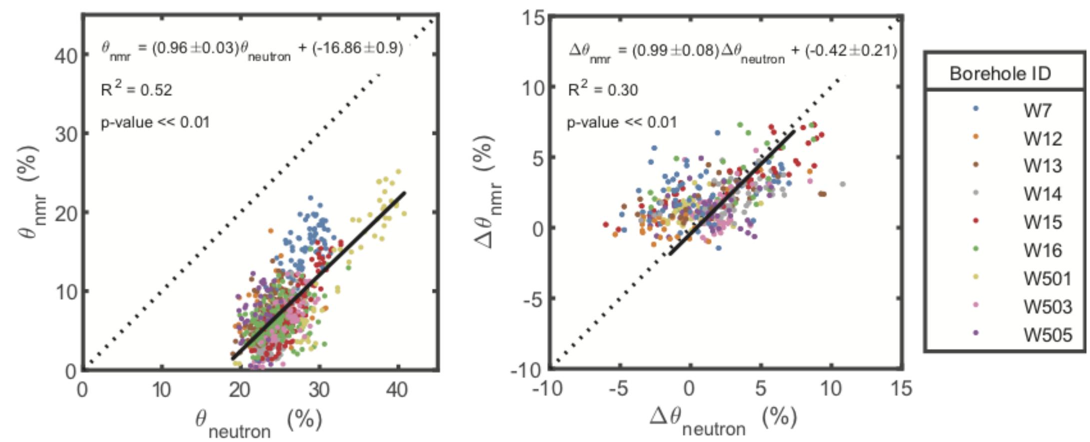

Figure 1.6 The relationship for θ and $\Delta\theta$ between paired NMR and neutron measurements. Color corresponds to borehole, the solid black line is the linear least-squares fit to the data, and the dotted line is the one-to-one line.

Patterns of Water Content and Dynamic Storage

The spatial patterns of θ (Figure 1.3) and $\Delta\theta$ (Figure 1.4) resolved by NMR and neutron are consistent, despite the disagreement in the magnitude of θ_{nmr} and $\theta_{neutron}$. Vertical profiles of θ_{nmr} and $\theta_{neutron}$ show loss of vadose zone water storage between the start and end of the summer dry season. Over the dry season, θ generally decreases or does not change (Figure 1.4). However, for small values of $\Delta\theta_{neutron}$ close to 0.01 m^3/m^3, the $\Delta\theta_{nmr}$ is typically below detection, and there are several depths where $\Delta\theta_{nmr}$ and $\Delta\theta_{neutron}$ have opposite signs. For example, at 7.5 m in W7, $\Delta\theta_{nmr}$ is negative, while $\Delta\theta_{neutron}$ is below detection (Figure 1.4). Such negative $\Delta\theta_{nmr}$ values are an erroneous result of measurement uncertainty. When actual water content changes are small, $\Delta\theta_{nmr}$ values are the result of subtracting measurement noise, and spurious negative values can occur. Fewer $\Delta\ \theta_{neutron}$ values are negative due to higher $\theta_{neutron}$ precision.

The spatial variability in water storage among and within wells is captured by both methods consistently. Both NMR and neutron measurements of θ and $\Delta\theta$ are sensitive to features at the meter and submeter scale (Figures 1.3 and 1.4). For example, both θ_{nmr} and $\theta_{neutron}$ in Figure 1.3c show an approximately 1 m thick interval of invariant, low water content centered at 7.7 m, and an approximately 1 m thick interval of dynamic, high water content centered at 3.3 m.

Storage estimates from NMR and neutron logging in this study are shown in Figure 1.7. Except for W16, $S_{dynamic}$ estimates from NMR and neutron agree within uncertainty (Figure 1.7a). In general, $S_{dynamic}$ measured via neutron tends to be greater than $S_{dynamic}$ measured via NMR (Figure 1.7a). This is due to the lower detection limit of neutron relative to NMR, such that small $\Delta\theta$ measurements are included in neutron $S_{dynamic}$ estimates, but not NMR (Figure 1.4).

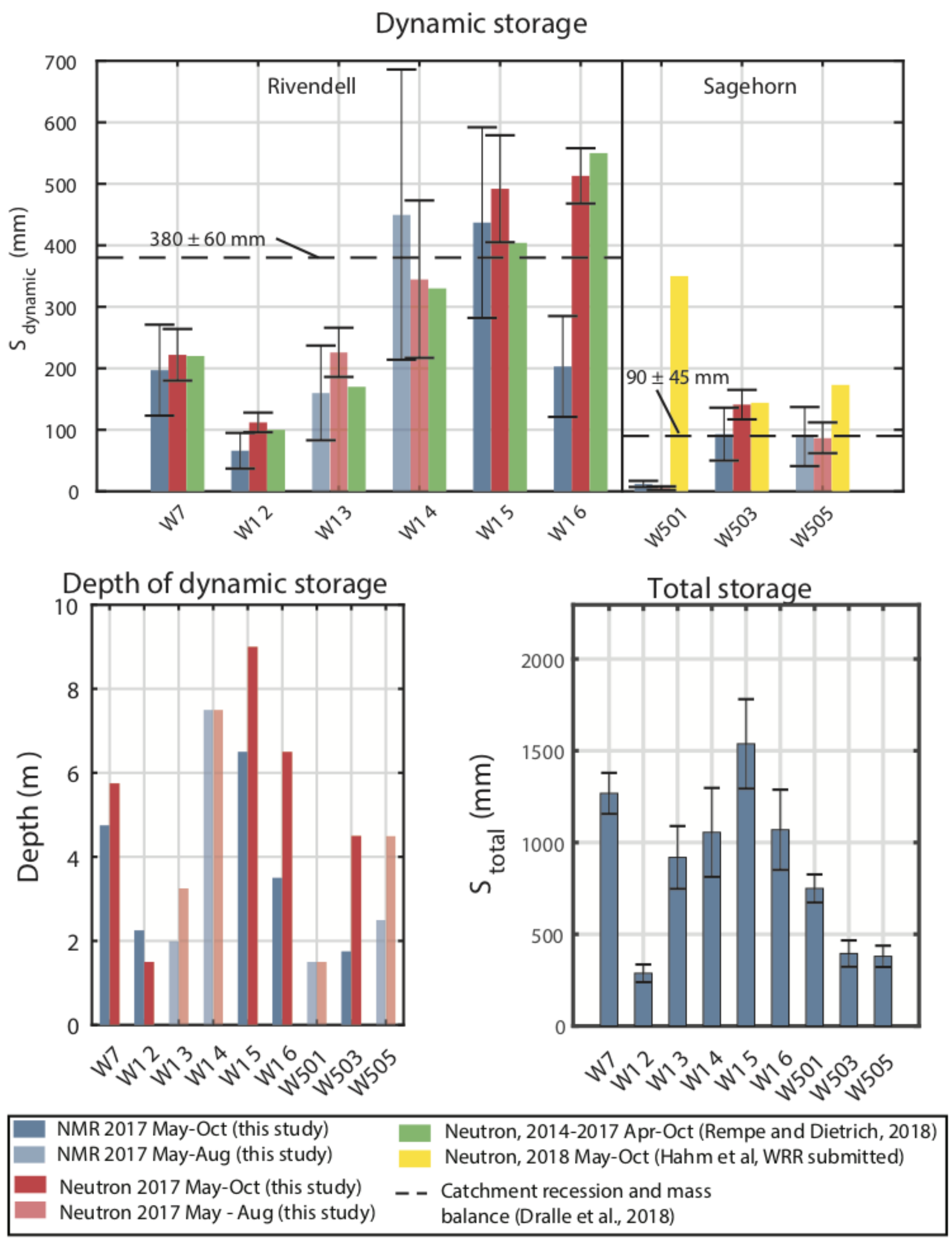

Dynamic storage
Rivendell
Sagehorn
380 ± 60 mm
90 ± 45 mm
S dynamic (mm)
W7
W12
W13
W14
W15
W16
W501
W503
W505
Depth of dynamic storage
Depth (m)
Total storage
S total (mm)
NMR 2017 May-Oct (this study)
NMR 2017 May-Aug (this study)
Neutron 2017 May-Oct (this study)
Neutron 2017 May - Aug (this study)
Neutron, 2014-2017 Apr-Oct (Rempe and Dietrich, 2018)
Neutron, 2018 May-Oct (Hahm et al, WRR submitted)
Catchment recession and mass balance (Dralle et al., 2018)

Figure 1.7 (a) Comparison of dynamic storage, (b) depth of dynamic storage, and (c) total storage from successive NMR (blue) and neutron (red) well logs. Error bars reflect the propagated uncertainty in θ and probe placement. Dynamic storage is calculated as the depth integral of $\Delta\theta$ between profiles logged in the wettest (May 2017) and driest well logs (August 2017 for wells W13, W14, W501, and W505 and October 2017 for wells W7, W12, W15, W16, and W501). Dynamic storage estimated in other studies are shown for reference (Dralle et al., 2018; Hahm et al., 2020). Depth of dynamic storage is the depth to which $\Delta\theta$ measurements are greater than measurement uncertainty. Total storage is calculated as the depth integral of water content measured in the May well logs, which represent wet conditions. Total storage is not estimated from neutron logs due to the lack of material-specific calibration.

The spatial patterns of water storage are consistent with what has been recorded in previous years at these sites (Hahm et al., 2020; Rempe & Dietrich, 2018). Previous studies similarly report dynamic water storage concentrated at shallow depths in the unsaturated zone, with little dynamic storage occurring at depths that are above and within the zone where the water table fluctuates. (Table S1 lists the depths where groundwater is encountered.) Our 2017 $S_{dynamic}$ measurements show general agreement with $S_{dynamic}$ measured by successive neutron well logs conducted by Rempe and Dietrich (2018) and Hahm et al. (2020) during other water years, except for W16 and W501 (Figure 1.7). At W16, $S_{dynamic}$ estimated via NMR is significantly lower than the $S_{dynamic}$ measured by neutron in different years of observation. At W501, the discrepancy between $S_{dynamic}$ measured in 2018 and 2017 is likely due to the timing of the 2018 survey, which occurred shortly after a rainfall event that transiently wetted the upper 1.5 m of the profile (Hahm et al., 2020). Dralle et al. (2018) report catchment average $S_{dynamic}$ of 380±60 mm for Rivendell (Elder Creek watershed) and 90 ± 45 mm for Sagehorn (Dry Creek watershed) using a combination of streamflow recession analysis and hydrologic mass balance techniques. These $S_{dynamic}$ estimates agree with the higher end of $S_{dynamic}$ observed in our borehole measurements. Estimates of the depth of dynamic storage from NMR and neutron generally agree to within 2–3 m, with neutron estimates generally being greater than NMR estimates due to the lower uncertainty of neutron measurements. Neutron estimates of S_{total} are roughly 2–5 times higher than NMR estimates due to $\theta_{neutron}$ being systematically greater than θ_{nmr}.

DISCUSSION AND CONCLUSIONS

Successive borehole NMR measurements capture the timing, spatial pattern, and magnitude of water content changes in the bedrock vadose zone at two seasonally dry field sites.

The agreement between NMR and neutron $\Delta\theta$ logging results indicates that borehole NMR is a reliable tool for monitoring dynamic storage in complex, heterogeneous bedrock vadose zones. We identify two important advantages to developing NMR for widespread use in the deep vadose zone. First, there is great potential for linking borehole NMR relaxation measurements to the hydraulic properties (such as water retention, e.g., Costabel & Yaramanci, 2011, 2013; Mohnke et al., 2014), of material tens of meters deep within the vadose zone and in rock. Such measurements are otherwise exceptionally difficult to obtain *in situ.* This detailed hydraulic information can serve to mechanistically link the physical structure of unsaturated bedrock systems to watershed functioning (Brantley, Brantley et al., 2017; Brantley, Lebedeva et al., 2017; Klos et al., 2018; Riebe et al., 2017). Second, compared to neutron logging—the current standard for direct monitoring in unsaturated bedrock—NMR is not associated with regulatory burdens, NMR can be deployed from the surface as well as via borehole tools, and the NMR signal does not require a material-specific nor casing-specific calibration to arrive at water content. The comparative ease of use of borehole NMR should result in improved monitoring of flow and transport in the bedrock vadose zone for applications associated with critical zone biogeochemical cycling, landscape weathering, and ecohydrology.

To obtain high-precision θ_{nmr} measurements with comparable uncertainty to other θ measurements, very low logging speeds are required. This presents a significant limitation. The precision of our borehole θ_{nmr} measurements (±0.014 m^3/m^3) based on repeat measurements, while on the order of some other water content measurement techniques such as TDR (Roth et al., 1990), is less than the precision of our neutron probe (±0.005 m^3/m^3) and less than the ±0.0005 m^3/m^3 neutron probe precision reported by Seyfried et al. (2001). Our θ_{nmr} uncertainty estimate is specific to this study because it represents our acquisition parameters, processing settings, and specific field conditions. In many monitoring locations, water content changes that were undetectable with NMR were detectable with neutron, which limits the extent to which water content measurements can be compared over space and time. In one monitoring location (W16), this discrepancy resulted in an underestimate of S_{dynamic} from NMR relative to neutron, 203 ± 82 (mm) versus 513 ± 45 (mm), respectively (Figure 1.7). Despite the limitations of NMR precision, our well logs led to reliable estimates of dynamic storage, suggesting that NMR could be applied reliably to a broad range of rock types and settings (Figure 1.7).

Several strategies could be considered to achieve higher precision estimates of dynamic storage with NMR. Uncertainty in our θ_{nmr} estimates is derived primarily from the multiexponential fit to the NMR decay curve. The estimate of θ_{nmr} is in principle independent of relaxation and is dependent only on the initial amplitude of the decay curve (Coates et al., 1999), but as is the case here, in practice θ is often estimated from the initial value of the multiexponential fit. This fit-derived θ can be larger than the initial decay curve amplitude if a significant fraction of water content is characterized by short relaxation times relative to the tool's echo-spacing time (Behroozmand et al., 2015; Dunn et al., 2002). In the vadose zone, water contents and relaxation times can be low, resulting in short decay curves with low signal/noise that inherently lead to fit-derived uncertainty in θ_{nmr}. To avoid errors that may arise due to the multiexponential fit, the average of the first decay curve amplitudes can be used as an alternative approach for estimating θ_{nmr}. However, when decay curves are primarily composed of short relaxation components relative to the pulse spacing, this approach will lead to greater underestimation of θ_{nmr} relative to actual θ. To combat NMR uncertainty, a high running average and low logging speed can be applied to arrive at a sufficiently high signal/noise ratio for monitoring small changes in low water contents. Additionally, using short repolarization times and measurement lengths can improve logging speed. To address variations in relaxation times in space and time within a given well log, we recommend initiating well logs with repeat measurements at representative locations and tuning logging parameters based on these site- and timing-specific results.

Our selection of regularization parameters presents another source of uncertainty for θ_{nmr} and thus non-dynamic storage, but not for $\Delta\theta_{nmr}$ or $S_{dynamic}$, because noise values are constant, and we use constant regularization factors across all data sets. To evaluate the impact of regularization factor on θ_{nmr}, we inverted our repeat measurements using a large range of regularization factors (Figure 1.8) and found that this effect is less than the θ_{nmr} uncertainty we report for repeat measurements (0.019 m^3/m^3). Our selection of 50, which is consistent with other studies (e.g., Kass et al., 2017), avoids overregularization or under regularization of our data.

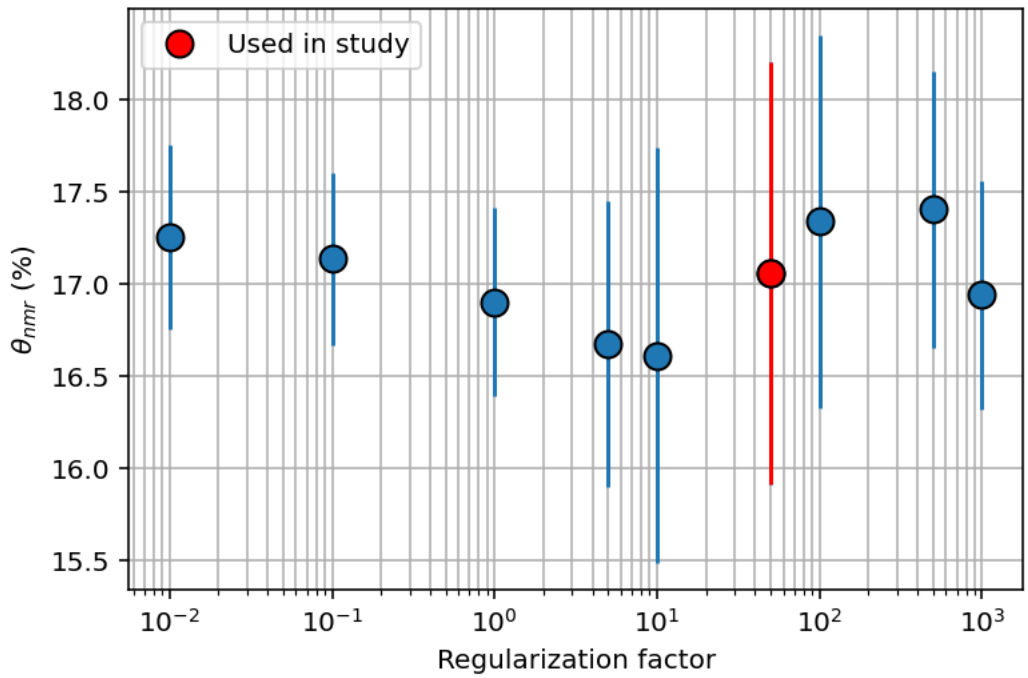

Figure 1.8 The impact of regularization factor on θnmr and its uncertainty for repeat measurements conducted at 10 m in monitoring borehole W7. Circles represent the mean value of three measurements and vertical bars represent the standard deviation. In this study, we use a regularization factor of 50.

The end-of-dry-season (seasonal minimum) θ_{nmr} is generally nonzero and in many locations can be as high as 10–15% (Figure 1.3). This indicates that there is a substantial volume of non-dynamic storage in the bedrock vadose zone. NMR measurements provide a conservative estimate of non-dynamic storage (S_{total} in Figure 1.7 less dynamic storage) for several reasons. First, there may be significant amounts of seasonally invariant water that is undetectable to NMR due to low relaxation times (<1 ms) below the echo-spacing-determined detection limit of the tool and are therefore excluded from θ_{nmr}. Pore diameters in the fine-grained matrix of our site are largely at the micron scale (Gu et al., 2020; Hahm et al., 2018). This means that water held in much of the matrix is likely to be characterized by relaxation times below the 0.5-ms echo-spacing time of the Dart (e.g., Lewis et al., 2013), rendering it undetectable and unaccounted for by our estimates of θ_{nmr}. Therefore, a significant fraction of the pore network may contain water outside of the detection range of our NMR instrument, and thus, θ_{nmr} is lower than actual θ. Second, in addition to pore size, multiple mechanisms may reduce θ_{nmr} relative to actual θ by enhancing relaxation times. These mechanisms include the presence of minerals that exhibit high magnetic susceptibilities on pore surfaces (Keating & Knight, 2008, 2010), residual water menisci with high surface area/volume ratios and therefore short relaxation times at low saturations (Mohnke et al., 2014), and biofilms (Kirkland et al., 2015). We therefore conclude that S_{total} And non-dynamic storage could be substantially larger than what is recorded by NMR.

There is considerable agreement between the spatiotemporal patterns of dynamic storage resolved by our NMR and neutron measurements. Both methods show that dynamic storage is concentrated at shallow depths, and we propose that the depth of dynamic storage (Figure 1.7) could represent an effective rooting depth. All or most of the dynamic storage reported here likely supplies transpiration for woody vegetation (Dralle et al., 2018; Hahm et al., 2020; Rempe & Dietrich, 2018). At both sites, roots in bedrock are observed in exposures (Hahm et al., 2019; Rempe & Dietrich, 2018), and at Rivendell, roots were observed to 16 m when drilling. The depth of dynamic storage is variable across the sites (Figure 1.7) such that neither site can be characterized by a single effective rooting depth. Patterns of dynamic storage diverge between methods at depths below the depth of dynamic storage where small changes occur that do not contribute significantly to dynamic storage.

The bedrock vadose zone at our sites is highly fractured, and we propose that our NMR monitoring provides evidence that unsaturated dynamic storage is dominantly—if not exclusively—held in fractures. The agreement in $\Delta\theta$ between paired NMR and neutron measurements, and the fact that NMR detects both dynamic and non-dynamic pore domains (because there is nonzero θ_{nmr} at the end of the dry season), shows that all dynamic storage occurs in pores detectable by NMR. Because water held in the fine-grained matrix at our sites is likely undetectable by our tool, virtually all dynamic water storages occur in larger, more interconnected pores, i.e., fractures. For the assumption that dynamic storage occurs exclusively within fractures, the range of $\Delta\theta_{nmr}$ of 0.108 m^3/m^3 (Figure 1.4) would represent the minimum fracture porosity. Future studies could use NMR relaxation measurements with measurements of surface relaxivity to evaluate the sizes and shapes of pores that host seasonally dynamic water (e.g., Mohnke et al., 2014).

Chapter 2: Using time-lapse borehole NMR relaxation measurements to investigate the relationship between weathering and water storage dynamics in the bedrock vadose zone

ABSTRACT

Methods for characterizing the *in situ* material properties that link water storage to weathering processes in bedrock vadose zones are lacking. Here, we apply time-lapse measurements of nuclear magnetic resonance (NMR) to the characterization of weathered bedrock because the saturation-dependance of NMR relaxation times is related to pore chemistry and structure. We use successive borehole surveys in deep wells across the deeply weathered Eel River Critical Zone Observatory "Rivendell" hillslope to relate NMR relaxation times to water storage dynamics driven by deeply rooted trees. We find that the low signal to noise ratio (SNR) associated with low water content and fast relaxation times in the vadose zone makes it challenging to apply conventional NMR interpretation approaches such as the full relaxation time distribution (RTD) or the logarithmic mean of the RTD. Instead, we leverage the sum of echoes (SE) to characterize relaxation times. The functional relationship between SE and water content serves as a proxy for the water retention function. We find that, at the same water content, more extensively weathered bedrock has faster relaxation times (lower SE) than less weathered bedrock. We suggest that the faster relaxation times observed in extensively weathered bedrock are caused by the accumulation of, due to weathering processes, oxides and clays with enhanced surface relaxivity. Further work is required to elucidate the role of pore structure. We also find that groundwater recharge can drive an increase an SE in the vadose zone without a detectable

water content increase, indicating that water is reconfigured in the pore space without a detectable change in water content. Thus, our in-situ documentation of SE and water content reveals, for the first time, a relationship between weathering, water retention, and water transport in the weathered bedrock vadose zone.

INTRODUCTION

The storage and transport properties of the bedrock vadose zone control transpiration and recharge in many catchments (McCormick et al. 2021; Grant and Dietrich 2017). These properties are closely related to the size and shape of pores (Blunt 2017). Pore structures in the bedrock vadose zone evolve over time due to weathering processes, which tend to increase water storage capacity (Riebe et al. 2017) and may convert otherwise ecohydrologically inert bedrock into "hospitable substrates for terrestrial ecosystems" (Graham et al. 2010; Riebe et al. 2017) if water storage becomes plant-accessible (Rempe and Dietrich 2018; Hahm et al. 2019; Hahm et al. 2022). Observations of pore structures, and how they evolve with weathering extent, therefore not only provide a mechanistic basis for modeling bedrock vadose zone water storage dynamics, but also provide a means of linking these mechanisms to weathering and ecological processes. However, *in situ* observations of pore mineralogy and structures in the bedrock vadose zone are rare. Laboratory analyses can provide detailed information about pore properties, but obtaining representative samples is difficult. For example, in some catchments, coring may be completely ineffective at preserving meso-scale fractures that dominate flow and storage properties. Methods are needed that provide *in situ* observations at the pore-scale throughout the weathering profile.

Borehole nuclear magnetic resonance (NMR) methods are a candidate for *in situ* characterization of the pore-scale properties of the bedrock vadose zone. Borehole NMR methods are well established for hydrocarbon and groundwater applications, where they are routinely used to measure porosity and the pore size distribution (PSD) of materials that are fully saturated with a single pore-fluid phase (Coates et al. 1999; Dunn et al. 2002; Behroozmand et al. 2015). Less routinely, NMR methods are used to characterize multiphase flow, although the interpretation is fundamentally different (Mohnke et al. 2015). In vadose zone applications where the pore-fluid phases are air and water, NMR measurements can be used to directly measure volumetric water content θ, but they cannot be used to directly estimate the PSD. Instead, the NMR signal is sensitive to the geometry of residual wetting layers (Blunt 2017) in pore corners, which changes with saturation (Costabel and Hiller 2021). The saturation-dependance of the NMR signal is therefore linked to water retention and it is closely related to water potential and pore shape. Understanding this link, and its application to vadose zone hydrology, is an active area of research (e.g., Hiller and Klitzsch 2018; Costabel and Hiller 2021; Falzone and Keating 2016b). An important result is that the saturation-dependance of NMR relaxation times can be used to parameterize the water retention function. So far, this approach has seen limited field application and has not been applied to weathered bedrock.

Here we conduct repeat, time-lapse borehole NMR well logging to measure NMR relaxation times as a function of θ to create "NMR characteristic curves" in different regions of the bedrock weathering profile underlying a well-studied hillslope called Rivendell. The NMR characteristic curve is analogous to the soil-water characteristic curve in that it is strongly affected by material properties such as texture and pore structure, and it is therefore related to hydraulic properties (Tuller and Or 2005). Note that the NMR characteristic curve, unlike the soil-water characteristic curve, is also affected by pore chemistry via surface relaxivity (Falzone and Keating 2016). Thus, comparison of the NMR characteristic curve can be used to infer differences in the physical and chemical properties of porous materials. Direct observations of bedrock vadose zone water storage dynamics via monitoring boreholes in the Rivendell hillslope have revealed that the vadose zone at this site is hydrologically stratified (Salve et al. 2012; Schmidt and Rempe 2020; Rempe and Dietrich 2018). Only the uppermost 2–8 m of the bedrock vadose zone hosts dynamic water storage. This region is interpreted to coincide with the root zone (Schmidt and Rempe 2020). Below the root zone, a thick (up to 20 m) region of the bedrock vadose zone does not host dynamic storage but it is important for rapidly transmitting water to recharge groundwater. We term this region the transmission zone. The root zone, being the uppermost portion of the weathering profile, is more extensively weathered than the deeper, less weathered transmission zone. Therefore, we hypothesize that NMR characteristic curves generated in the root zone will be different from NMR characteristic curves generated in the transmission zone.

To overcome low signal-to-noise ratio (SNR) associated with low water contents and fast relaxation times, we use the sum of echoes (SE) approach for characterizing relaxation times (Chen 2000), which provides several advantages for this application compared to more conventional approaches such as the full relaxation time distribution (RTD) or the logarithmic mean of the RTD (T_{2ml}). SE is proportional to the product of θ and the mean relaxation time ($T_{2,m}$)

(Eq 2.1) $$SE = (1/T_e)\theta \cdot T_{2m}$$

where T_e is the echo spacing (Chen 2000). Here, we plot SE as a function of θ to generate "NMR characteristic curves" in the root zone and the transmission zone. These curves are then used to investigate the relationship between bedrock weathering and plant-available water storage.

SITE DESCRIPTION AND HILLSLOPE HYDROGEOLOGY

Borehole NMR measurements were made in three boreholes drilled into a steep, forested, north-facing hillslope in the Elder Creek watershed in northern California called Rivendell. The hillslope is mantled with thin soils (up to 0.5 m thick), which overlie deeply weathered bedrock that ranges from nearly 30 m at the ridge top to 4 m near the channel. The contact between weathered and fresh bedrock is interpreted to be a strong hydraulic conductivity contrast above which a seasonally dynamic water table forms. The catchment, including Rivendell, is underlain by nearly vertically dipping argillite bedrock with minor sandstone interbeds in the Coastal Belt of the Franciscan Formation. Average annual precipitation is ~2000 mm, but there is significant variability (Hahm et al. 2019). Nearly all precipitation occurs in a 5–6 month period in the winter. The catchment supports an old-growth mixed broadleaf-needleleaf evergreen forest dominated by Douglas fir (Pseudotsuga menziesii) on north-facing slopes. The region has a Mediterranean climate of warm dry summers and cool wet winters. The peak incoming solar radiation occurs after the last significant wet season precipitation event, which typically occurs in May. Transpiration is sustained throughout the dry season by water storage in the root zone (Rempe and Dietrich 2018; Hahm et al. 2019) which coincides with the upper part of the bedrock vadose zone, up to ~10 m (Schmidt and Rempe 2020).

The hydrogeology of the hillslope is well documented (Salve et al. 2012). The groundwater table fluctuates seasonally, and the vadose zone, which is more than 20 m thick at the ridge, is dominated by weathered bedrock. No overland flow occurs at the site and saturation or lateral flow within soils or shallow weathered bedrock has not been documented. Monitoring with time-lapse neutron well logging has shown that dynamic water storage (up to ~500 mm) occurs in the soil and uppermost 2–8 m of the bedrock vadose zone. This region is interpreted to coincide with the root zone (Schmidt and Rempe 2020). Water storage in the root zone is rapidly replenished by infiltration in the first months of the winter wet season (characterized by the advance of a wetting front), and slowly depleted by transpiration during the summer dry season (with no associated drying front). The thickness of the root zone, defined as the depth of dynamic storage, is consistent year-to-year. Below the root zone, a thick (up to 10 m) region of the bedrock vadose zone does not host dynamic storage, but it is important for transmitting water to recharge groundwater. We term this region the transmission zone. Water contents measured with well logging in the transmission zone do not fluctuate seasonally. Transmission zone water content tends to be lower than water contents observed in the root zone, except during the driest conditions when root zone water contents has been, in some boreholes, measured to be lower (Schmidt and Rempe 2020). Groundwater responds very rapidly during the first major storms, long before vadose zone water storage is detected. This is interpreted to be the result of a kinematic wave that is transmitted through the vadose zone, and it is consistent with a pore network composed of fractures (Salve et al. 2012). Groundwater tends to rise in episodic jumps associated with precipitation events during the wet season, and to fall monotonically during the dry season.

METHODS

Borehole NMR logs were acquired in two deep wells W14 and W15 (Figure 2.1) with a Dart NMR Logging System (Vista Clara, Inc., Mukilteo, Washington, USA). These boreholes were selected for analysis in this study because they intersect locations where the perennially unsaturated vadose zone is thickest, i.e., the water table does not rise above ~20 m from the land surface (Figure 2.1). This means that these boreholes intersect both a thick root zone (~8 m) and a thick transmission zone (~12 m), which enables the maximum number of well logging observations to be obtained in, and to be used to compare, these two regions. We acquired six well logs over the course of a year from May 2017 to March 2018 (Figure 1). This spans a period of drying (May to October) and a period of wetting (October to March). Measurements were taken every 0.25 m. The volume of investigation (VOI) of the Dart is two cylindrical shells of height 0.23 m, thickness 1–2 mm, and radius 6.5 or 7.6 cm (determined by operational frequency), centered on the central axis of the tool (Walsh et al., 2013). For reference, the total VOI of the Dart (~400 cm^3, the sum of the volume of the two shells) is comparable to the low end of the range of VOIs of TDR and capacitance soil moisture sensors (200–2,000 cm^3) and is 2 to 3 orders of magnitude smaller than the range provided by neutron probes (34,000–270,000 cm^3, Campbell et al. 2022). Estimates of dynamic water storage derived from NMR well logging with the Dart have been shown to agree with estimates derived from neutron well logging at Rivendell, despite the differences in volume of investigation between the methods (Schmidt and Rempe 2020). This agreement suggests that the NMR VOI is larger than the representative elementary volume for water content at Rivendell. The shallowest logged depth is 1.5 m, which is within bedrock and below soils in all boreholes. Acquisition parameters are identical to those used by Schmidt and Rempe 2020. Each NMR decay curve in the dataset was acquired with the Carr-Purcell-Meidboom-Gill pulse sequence at two operational frequencies near 420 and 480 kHz, respectively, with sixty echoes and an echo spacing of 0.5 ms. These settings result in a measurement duration of 0.3 s. Decay curve data were stacked 168 times, and each stack was separated by a repolarization time (or wait time) of 0.15 s. Before each campaign, the system was calibrated in a shielded water sample in the lab. The NMR data were processed using commercial software (JavelinProcess_v4.4 and JavelinInterpret_v1.8, Vista Clara, Inc.). All stacks, stages, and frequencies associated with each depth interval were combined, and the resulting NMR decay curve was fit with a multi-exponential decay function determined via a nonnegative least squares inversion algorithm with second-order Tikhonov regularization using the default software regularization factor of 50.

We used data that minimizes reliance on inversion. To estimate θ, rather than use the value of the multi-exponential fit, we take the average of the first three echoes in the decay-curve. Decay curve noise level was calculated as the root mean squared of the residuals of the decay curve and the fit. Decay curve SNR was calculated as the ratio of θ and noise level. SE is the sum of the decay curve. The SE noise level is the root mean squared of the residuals of the cumulative sum of the decay curve and the cumulative sum of the fit. SE SNR is calculated as the ratio of SE and SE noise level. T_{2ml} is an output of the software.

RESULTS

Data quality

We compare the performance of SE, θ, and T_{2ml} for reflecting water storage dynamics at our site in Figure 2.1. The acquisition parameters used to collect this NMR dataset were optimized for water content monitoring (Schmidt and Rempe 2020) and not for relaxation time analysis. We report the limitations that result from this here.

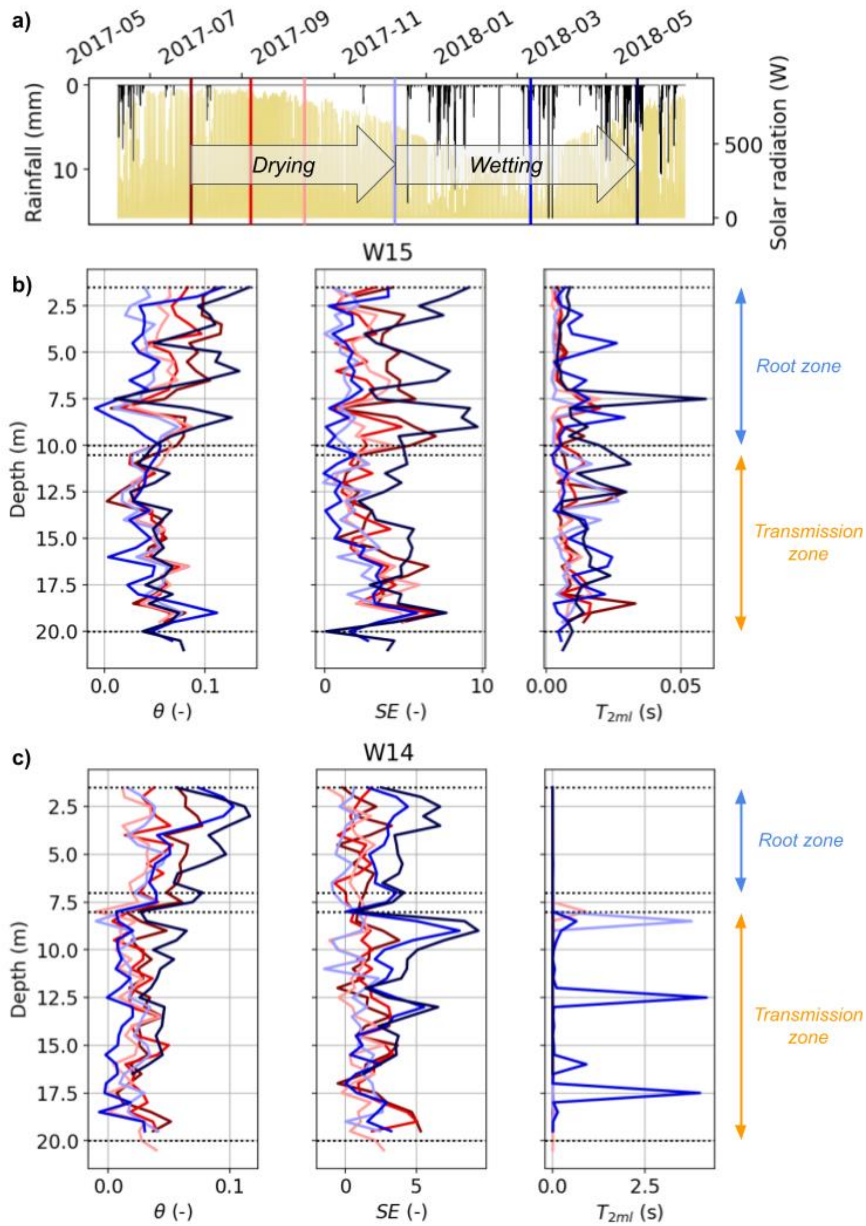
a)
2017-05
2017-07
2017-09
2017-11
2018-01
2018-03
2018-05
Rainfall (mm)
Solar radiation (W)
Drying
Wetting
W15
b)
Depth (m)
θ (-)
SE (-)
T2ml (s)
Root zone
Transmission zone
W14
c)
Depth (m)
θ (-)
SE (-)
T2ml (s)
Root zone
Transmission zone

Figure 2.1. Time series of (a) the timing of surveys, rainfall, and total solar radiation measured at the Elder Creek watershed. Comparison (b) of time-lapse θ, SE, and T_{2ml} well logs. Horizontal dashed lines delineate the extent of the root zone and transmission zone. Colored vertical lines in (a) mark the timing of the well logs in b and c.

The decay curves in this study have low SNR (Figure 2.2 and 2.3a). The average SNR of decay-curves is 1.8 ± 1.15. Low SNR is due to high noise levels relative to moisture conditions in the bedrock vadose zone during our study. The average noise level of decay curves is 0.031 ± 0.003, which is close to half the mean θ signal of 0.06 ± 0.04 m^3/m^3. The variability of θ was greater than the variability of noise, therefore SNR is controlled by water content.

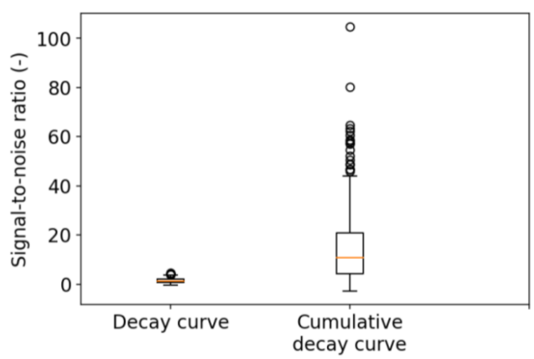

Figure 2.2. Boxplots of decay curve and cumulative decay curve signal-to-noise ratios for all measurements in this study.

The SNR of cumulative decay curves is on average about 50% greater than the SNR of raw decay curves (Figure 2.2 and 2.3b). The average SNR of cumulative decay curves is 15 ± 14. The improvement in SNR of cumulative decay curves can be observed in Figure 3a and 2.3b. Average $SE(t)$ noise level is 0.2 ± 0.1, while average SE signal is 2.9 ± 2.4.

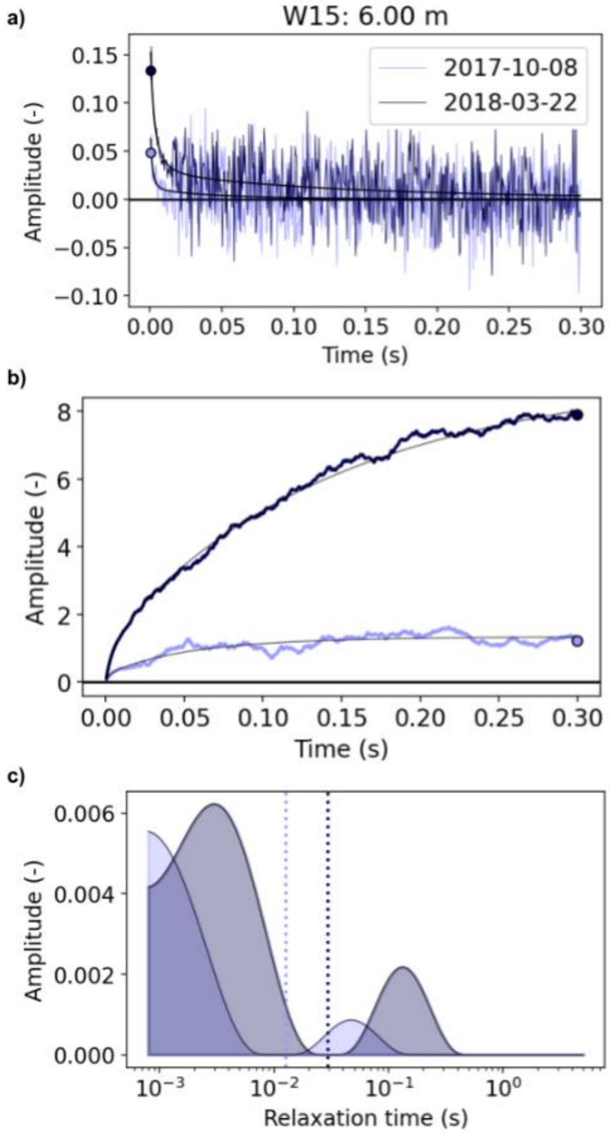

Figure 2.3. Examples of typical (a) decay curves, (b) cumulative decay curves, and (c) relaxation time distributions for NMR measurements made at dry (light blue) and wet (dark blue) conditions. These measurements were obtained in the same monitoring location in W15. Vertical lines in (c) are the T_{2ml} values. The increase in SNR of the cumulative decay curves relative to the unsummed decay curves can be observed by comparing (a) and (b). Note the shift to faster relaxation times between wet and dry conditions in (c).

At low θ (less than ~0.05 m^3/m^3, i.e., at low SNR) T_{2ml} values tend to increase (Figure 2.4). Physically, T_{2ml} should decrease with decreasing θ in response to air invading pore centers and the shrinking of wetting layers (Mohnke 2015). By comparison, SE values decrease with decreasing θ, suggesting that spuriously high T_{2ml} values at low θ are an artifact introduced in the inversion process when SNR is low. T_{2ml} well logs are severely affected by these artifacts—particularly in the transmission zone (where θ values tend to be perennially low), but also in the root zone when conditions are dry (Figure 2.1). These artifacts make interpreting T_{2ml} well logs challenging without further processing. For this reason, we do not use T_{2ml} to characterize NMR relaxation times in this study and focus on SE to characeterize NMR relaxation times instead.

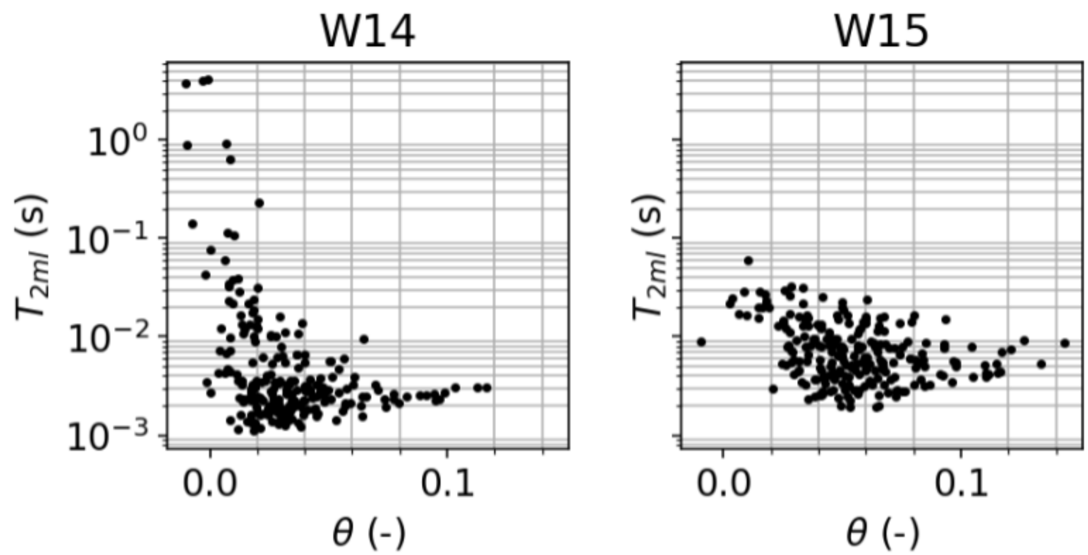

Figure 2.4. Scatterplots of mean log T_2 values (T_{2ml}) as a function of volumetric water content (θ). As water contents values decrease (θ < ~0.05 m3/ m3), T_{2ml} values increase, an aphysical artifact resulting from low decay curve SNR.

Many decay curves that were collected in wet conditions are incomplete, i.e., the NMR signal did not entirely decay to zero by the end of the measurement (0.3 s). This incompleteness can be seen clearly in cumulative decay-curves, even when it is not obvious in the unsummed decay curve (Figure 2.3). Incompleteness does not affect the θ estimate, but it does result in artificially low SE. This means that many of the SE values in this study, particularly the highest values, are underestimates of the SE value that would have been obtained had the measurement duration been longer than 0.3 s.

There is evidence that our SE well logs have increased contrast relative to θ, but the difference is not qualitatively obviously in time-lapse well logs. Contrast in this context is the magnitude of change of the measurements (i.e., SE or θ) in response to a change in *in situ* moisture content. The coefficient of variation (CV) is a useful proxy for comparing the contrast of different monitoring products because it is a standardized measure of variability, and variability of SE and θ values is controlled by their sensitivity to changes in water content. The CV of SE in the root zone, where water content changes are largest and, therefore, where contrast should be most strongly expressed, is roughly two times higher than the CV of θ (Table 1). Higher root zone CV is consistent with SE having higher contrast than θ. However, this increase in contrast is not obvious in plots of the time-lapse well logs (Figure 2.1). Presumably, SE contrast would be higher had measurement durations been longer.

Borehole	Root zone $\boldsymbol{\theta}$ CV	Root zone $\boldsymbol{SE}$ CV
W15	0.4	0.7
W14	0.5	1

Table 1. Comparison of root zone volumetric water content (θ) and sum of echoes (SE) contrast, using the coefficient of variation (CV) as a metric.

Timing of groundwater table rise, $\boldsymbol{\theta}$ and $\boldsymbol{SE}$ increase

The temporal dynamics of θ and SE are generally coupled (see Equation 2.1) such that a change in θ is associated with a corresponding change in SE. This is the case for observations in the root zone, but we note one important exception for transmission zone observations: in both W14 and W15, when the groundwater table in the borehole is rising, we observe a sharp increase in average transmission zone SE (percent change of 128 and 118 for W14 and W15, respectively) without a corresponding large change in average transmission zone θ (percent change of -51 and 17 for W14 and W15, respectively) (Figure 2.5). Effectively, average transmission zone SE increases before average transmission zone θ increases during the wet season. This initial increase in average SE happens in W14 earlier than in W15, but in both wells the timing of the initial average SE increase corresponds with a rising water level in the borehole, which occurs earlier in W14 than in W15. An increase in SE without a change in θ implies that T_{2m} changed without a detectable change in water volume.

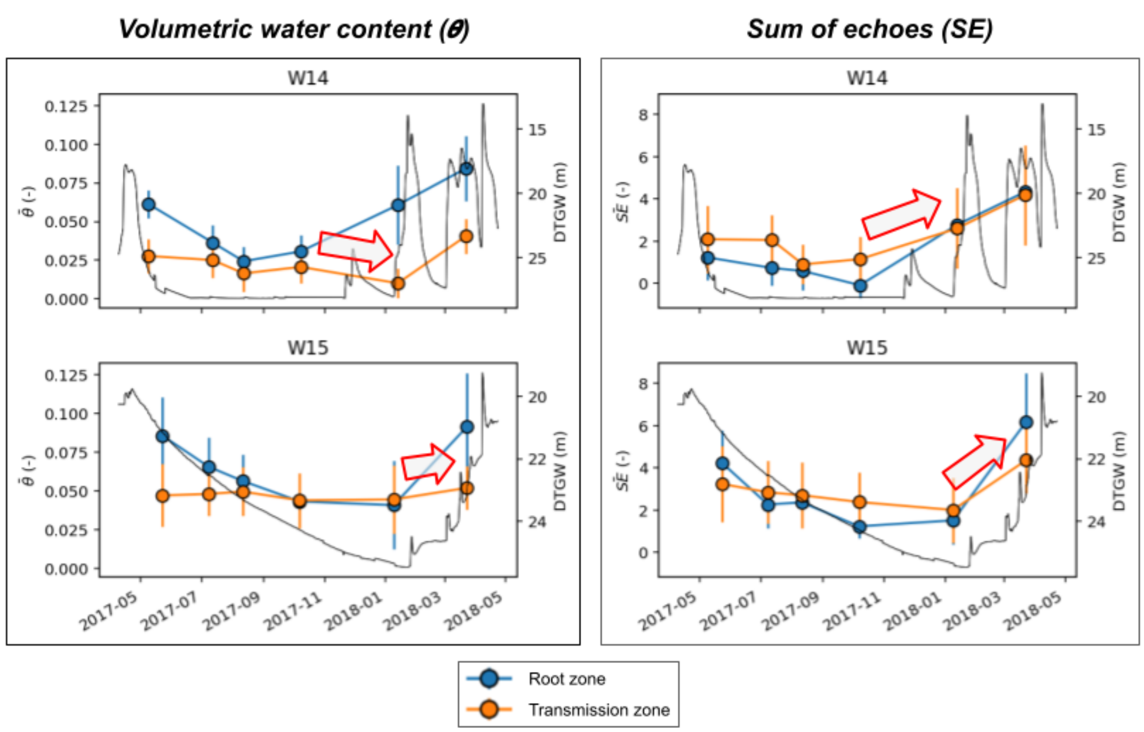

Figure 2.5. Time-series of average root zone (orange) and transmission zone (blue) volumetric water content ($\bar{\theta}$) and sum of echoes ($\overline{SE}$) in W14 and W15, superimposed on time-series of the water table in each borehole. Red arrows indicate when transmission zone $\bar{\theta}$ and $\overline{SE}$ changes diverge. Transmission zone $\overline{SE}$ increases without a corresponding change in transmission zone $\overline{SE}$, and the timing of this increase coincides with the rising groundwater level. Bars represent the standard deviation of measurements in the zone.

NMR characteristic curves

To test the hypothesis that root zone and transmission zone NMR characteristic curves are different, NMR characteristic curves representing the root zone and the transmission zone were created for measurements in W14 and W15 (Figure 2.6). We make four key observations regarding these differences. First, root zone NMR characteristic curves are different from transmission zone NMR characteristic curves. This means the mean relaxation times in root zone material are different from transmission zone material. Second, the characteristic curves in both W14 and W15 show a consistent difference between the root zone and the transmission zone across the two wells. This means that a similar transition in SE saturation-dependence with depth occurs in two different parts of the hillslope. Third, the average SE value at a given θ is lower in the root zone than in the transmission zone. This means that, in these boreholes, the T_{2m} time of root zone material is lower than the T_{2m} value of transmission zone material over the range of water contents measured in the study. Fourth, the slope of the root zone characteristic curve is lower than the slope of the transmission zone characteristic curve. This means that for the same change in θ, the change in root zone SE is less than the change in transmission zone SE. Therefore, compared to the root zone, the range of SE in the transmission zone is high relative to the range in θ. Another consequence is that while the maximum θ attained in the root zone is significantly higher than the maximum θ attained in the transmission zone, maximum root zone and transmission zone SE are similar.

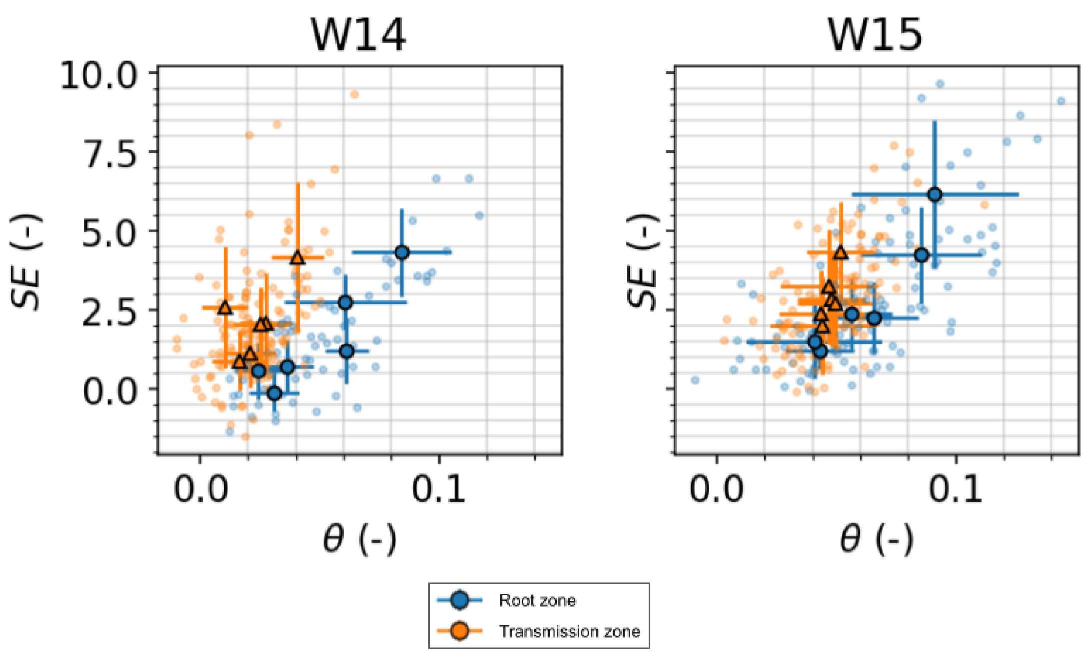

Figure 2.6. NMR characteristic curves of the root zone (orange) and transmission zone (blue). Small markers are individual measurements, large markers are the average of all measurements in the zone for a well log, and bars are the standard deviation.

DISCUSSION AND CONCLUSIONS

Weathering extent is associated with shorter mean relaxation times for a given water content

We confirm our hypothesis that the NMR characteristic curves for the root zone and transmission zone are different (Figure 2.6). This hypothesis is based on the expectation that weathering extent influences NMR relaxation times. While very few studies have explicitly investigated how weathering effects NMR relaxation times, there is an expectation that changes in mineralogy and pore structure associated with weathering will impact the NMR response. NMR relaxation times are sensitive to the surface-to-volume ratio of pore water and to the mineralogy of pore walls via surface relaxivity (Coates, Xiao, and Prammer 1999; Dunn, Bergman, and LaTorraca 2002; Behroozmand, Keating, and Auken 2015). Both parameters can be expected to be strongly influenced by weathering. For example, numerous studies have shown that surface relaxivity increases with increasing concentration of ferrous oxides (Keating and Knight 2007; Foley, Farooqui, and Kleinberg 1996; Bryar, Daughney, and Knight 2000; Bryar and Knight 2002; Keating and Knight 2008, 2010; Falzone and Keating 2016a), and clays (Saidian and Prasad 2015), both of which are generated by weathering. Likewise, weathering processes change the size and shape of pores. At Rivendell, both the concentration of ferrous oxides and the structures of pores have been shown to evolve with weathering/depth (Gu et al. 2020). Therefore, we expect the shallower, more weathered root zone material to generate NMR characteristic curves that are distinct from the deeper, less weathered transmission zone. This is confirmed by our results (Figure 2.6), which demonstrates that time-lapse borehole NMR measurements of water storage dynamics can be used to infer differences in the material properties of the bedrock vadose zone driven by weathering.

The vertical differences in our NMR characteristic curves allow us to infer the effect of weathering on NMR relaxation times. At our site, which is underlain by nearly vertically dipping turbidite deposits dominated by argillite, vertical changes in material properties are primarily the consequence of the development of the weathering profile (whereas at sites underlain by layer-cake geology, bedding may exert a stronger control on the depth-dependance of material properties). Our NMR characteristic curves (Figure 2.6) show that, for a given θ, the T_{2m} of the shallower—and therefore more extensively weathered—root zone is shorter than in the deeper, fresher transmission zone. From this, we conclude that weathering processes tend to shorten NMR relaxation components at our site. A detailed mechanistic explanation for this phenomenon is beyond the scope of this study. However, we note that a reduction in T_{2m} for a given θ is consistent with an increase in ρ, which could plausibly be generated by weathering processes that increase the concentration of ferrous oxides and secondary clays. Likewise, changes in pore structure associated with weathering could also contribute to decreased T_{2m}, but the relationship between weathering, pore structure, and NMR relaxometry of unsaturated media is not straightforward. This is because relaxation times are dependent on both pore size and pore shape, both of which can plausibly change due to weathering, but the dependance of T_{2m} on these parameters can work in opposite directions. For a partially saturated porous media at a fixed water potential, SE decreases with decreasing pore size, but it increases with increasing pore angularity (e.g., Costabel and Hiller 2021). Therefore, pore angularity may play a role in our results, but data are not available to evaluate this. Studies documenting the relationship between pore size, pore angularity, and weathering extent are needed to elucidate whether the pore structure of weathered material is associated with enhanced ρ for a given water content.

The agreement in the depth patterns between NMR characteristic curves generated in W14 and W15 (Figure 2.6) suggests that the same general transitions in material properties with depth occur in both locations. Drilling has shown that W14 and W15 are both dominated by argillite with some sandy interbeds located at shallow depths in W15 (Rempe 2016). We therefore we expect similar transitions in material properties with depth to occur in both locations. This is supported by our characteristic curves (Figure 2.6).

Recharge events and SE dynamics in the transmission zone

Large changes in SE are not accompanied by changes in θ in the transmission zone when groundwater recharge is occurring (Figure 2.5). Typically, we expect changes in vadose zone relaxation times to be accompanied by changes in water content because changing the saturation of pores changes the surface-to-volume ratio of wetting layers (Mohnke 2015; Hiller and Klitzsch 2018; Costabel and Hiller 2021). This association between θ and SE is what is observed between most well logs in this study, and it is why the NMR characteristic curves in Figure 2.6 are well-approximated by lines (ΔSE is proportional to $\Delta\theta$). However, in the transmission zone of each borehole, the one survey that was conducted during the wet season when groundwater recharge was occurring shows a percent change in mean SE that is more than an order of magnitude larger than the corresponding percent change in mean θ (Figure 2.5). It is well documented that at our site the bedrock vadose zone can transmit pressure rapidly without detectably changing water storage (Salve et al., 2012). When water storage increases, an increase in water pressure is transmitted throughout the bedrock vadose zone. In the transmission zone, this results in a change in water configuration which could plausibly generate a detectable change in NMR T_{2m}. An increase in water pressure will necessarily result in a change in θ, but depending on pore geometry, this change could be small enough to be undetectable to neutron or NMR. NMR observations in fractured settings could provide constraint on flow and transport parameterization in model frameworks.

Conclusions

This study presents time-lapse measurements of changes in water content (Chapter 1) and relaxation times (Chapter 2) from borehole NMR measurements made in the bedrock vadose zone. We summarize the principal conclusions of the study here.

NMR-derived estimates of water content θ_{nmr} (which ranged from 0% to 30%; mean θ_{nmr} was 2%) were lower than paired estimates independently derived from neutron measurements $\theta_{neutron}$ (which ranged from 20% to 40%; mean $\theta_{neutron}$ was 30%) by a constant value (Figure 1.3 and 1.6). We find that, roughly,

$$\theta_{nmr} = \theta_{neutron} - 0.2.$$

We suggest two factors contribute to the offset in water content estimated by the two methods. First, a certain fraction of true water content is not detectable by the NMR tool (the water content components with the smallest relaxation times, i.e., the smallest wetting layers), but all true water content is detectable by the neutron tool. Therefore, we expect NMR-derived estimates of water content to be a fraction of neutron-derived estimates. Second, the calibration relation for the neutron tool was developed using sand as the solid phase. Therefore, we expect a certain amount of offset between neutron-derived estimates of “sand-equivalent” water content and true water content in the bedrock vadose zone.

The agreement in slope between θ_{nmr} and $\theta_{neutron}$, suggests that NMR is a viable candidate for developing calibration relationships to convert neutron counts to water contents. In general, it is difficult to obtain a neutron calibration relationship that generates accurate estimates of absolute water content (it is much easier to obtain accurate estimates of water content change) for the entire subsurface, which is heterogenous. Therefore, the ability to calibrate against NMR measurements made in bedrock *in situ* is an advantage unique to borehole NMR.

We show that NMR well logging provides a dependable, repeatable lower-bound for total water storage capacity. We present NMR-derived estimates of total wet-season water storage (which range from 250 mm to 1500 mm) in the bedrock vadose zones at our sites (Figure 1.7).

NMR- and neutron-derived estimates of water content change ($\Delta\theta$ estimates derived from both methods ranged from 0% to 5%; mean $\Delta\theta$ was 2%) agree (Figure 1.4 and 1.7). We find that, roughly,

$$\Delta\theta_{nmr} = \Delta\theta_{neutron}.$$

This agreement is important for establishing the ability for borehole NMR to detect and accurately measure water content changes *in situ* in the bedrock vadose zone despite the small volume of investigation, detectability-limitation, and low signal-to-noise ratio inherent to the borehole NMR method. Future studies are needed to determine over what range of subsurface conditions this relationship holds.

The agreement between NMR- and neutron-derived estimates of water content change shows that all seasonally exchanged bedrock water storage is detectable by NMR at our sites. Because water held in the fine-grained bedrock matrix at our sites is not detectable by our NMR tool, we argue that, because all seasonally exchanged water was detectable, all seasonally exchanged water must be hosted by fractures. Under that assumption, our estimates of $\Delta\theta$ represent lower bounds on fracture porosity.

Low SNR is the primary challenge to detecting water content changes with borehole NMR. For water content monitoring, we recommend using a high running average, especially in dry conditions (water content less than 5%). If the relaxation time distribution is not important for a particular application, shortening the measurement duration can increase logging speed without affecting the water content estimation.

We find that the summation of echoes (SE) approach for monitoring water content and relaxation time changes is particularly useful for time-lapse vadose zone applications where water contents, and therefore SNR, are inherently low. The summation of the decay curves in this study resulted in a 50% increase in SNR, and SE measurements showed a twofold increase in contrast compared to θ (Figure 2.2). Unlike $T_{2,ml}$ measurements, which were aphysically high at water contents less than ~5%, SE measurements are not derived from the inversion-derived relaxation time distribution and therefore are not afflicted by inversion artifacts associated with low SNR (Figure 2.4). The SE approach provides a fast, convenient, and robust method for characterizing water content and relaxation time changes. With longer measurement durations and decay curves with higher SNR than were used in this study, we anticipate that the advantages of SE would be even more pronounced.

We show evidence that SE is sensitive to the kinematic transmission of pressure associated with recharge events (Figure 2.5). During a winter recharge event, we observed a percent change in average transmission zone SE that was more than two orders of magnitude larger than the attendant percent change in θ. This implies a reconfiguration of pore-water without a change in water content. Future studies are needed to elucidate this phenomenon.

We demonstrate that "NMR characteristic curves," which show the functional relationship between NMR relaxation times and water content, can be used to infer differences in material properties. Root zone and transmission zone measurements produce distinct NMR characteristic curves (Figure 2.6). We expected this result due to the known differences in weathering extent between the root zone and the transmission zone. Bedrock weathering affects relaxation times by changing the size, shape, and surface relaxivity of pores. With independent measurements of surface relaxivity or water potential, and with NMR measurements with higher SNR than obtained in this study, NMR characteristic curves could be used to parameterize the water retention function of deep vadose zones composed of bedrock.

We find that bedrock weathering extent is associated with faster relaxation times (Figure 2.6). For the same water content, average transmission zone SE is higher (slower relaxation times) than average root zone SE (faster relaxation times). In wet conditions, we observed a mean transmission zone SE that was eight times higher than mean root zone SE. We attribute the faster relaxation times in the root zone to the higher concentration of clays and oxides present in that region due to more extensive weathering. Future work is required to determine whether the effect of weathering on pore shape contributes to faster relaxation times. Based on our findings, we hypothesize that, like soil-water characteristic curves, NMR characteristic curves are related to permeability: we expect that low permeability materials, such as clays, will generally exhibit faster relaxation times than high permeability materials, such as sands, for the same water content. Future studies are needed to confirm this hypothesis, but if it proves to be true, then NMR monitoring in the vadose zone provides a means for rapidly evaluating the relative permeability of subsurface materials *in situ*.

The work presented here establishes borehole NMR well logging as a viable method for *in situ* vadose zone monitoring and characterization. We anticipate that NMR systems will be increasingly applied to vadose zone hydrogeologic problems, particularly in thinly soiled catchments underlain by a thick vadose zone composed of bedrock.

References

Babaeian, E., Sadeghi, M., Jones, S.B., Montzka, C., Vereecken, H. and Tuller, M., 2019. Ground, proximal, and satellite remote sensing of soil moisture. Reviews of Geophysics, 57(2), pp.530-616.

Behroozmand, A.A., Keating, K. and Auken, E., 2015. A review of the principles and applications of the NMR technique for near-surface characterization. Surveys in geophysics, 36(1), pp.27-85.

Bell, J. P., and Institute of Hydrology (Great Britain). 1987. Neutron Probe Practice.

Black, Charles Allen. 1965. Methods of Soil Analysis: Physical and Mineralogical Properties, Including Statistics of Measurement and Sampling. Part 1.

Blunt, M.J., 2017. Multiphase flow in permeable media: A pore-scale perspective. Cambridge university press.

Brantley, S.L., Lebedeva, M.I., Balashov, V.N., Singha, K., Sullivan, P.L. and Stinchcomb, G., 2017. Toward a conceptual model relating chemical reaction fronts to water flow paths in hills. Geomorphology, 277, pp.100-117.

Bryar, T.R. and Knight, R.J., 2002. Sensitivity of nuclear magnetic resonance relaxation measurements to changing soil redox conditions. Geophysical Research Letters, 29(24), pp.50-1.

Bryar, T.R., Daughney, C.J. and Knight, R.J., 2000. Paramagnetic effects of iron (III) species on nuclear magnetic relaxation of fluid protons in porous media. Journal of magnetic resonance, 142(1), pp.74-85.

Carrière, S.D., Chalikakis, K., Danquigny, C., Davi, H., Mazzilli, N., Ollivier, C. and Emblanch, C., 2016. The role of porous matrix in water flow regulation within a karst unsaturated zone: an integrated hydrogeophysical approach. Hydrogeology Journal, 24(7), pp.1905-1918.

Campbell, G. S., Campbell, C. S., Cobos, D. R., Brown, D., Crawford, L. B., Rivera, L., & Chambers, C. (2022). Soil moisture sensors—How they work. Why some are not research-grade. Metergroup.com. Retrieved August 1, 2022, from https://www.metergroup.com/en/meter-environment/measurement-insights/tdr-fdr-capacitance-compared

Coates, G.R., Xiao, L. and Prammer, M.G., 1999. NMR logging: principles and applications (Vol. 234). Houston: Haliburton Energy Services.

Costabel, S. and Hiller, T., 2021. Soil hydraulic interpretation of nuclear magnetic resonance measurements based on circular and triangular capillary models. Vadose Zone Journal, 20(2), p.e20104.

Costabel, S. and Yaramanci, U., 2011. Relative hydraulic conductivity in the vadose zone from magnetic resonance sounding—Brooks-Corey parameterization of the capillary fringe. Geophysics, 76(3), pp.G61-G71.

Costabel, S. and Yaramanci, U., 2013. Estimation of water retention parameters from nuclear magnetic resonance relaxation time distributions. Water Resources Research, 49(4), pp.2068-2079.

Dralle, D.N., Hahm, W.J., Rempe, D.M., Karst, N.J., Thompson, S.E. and Dietrich, W.E., 2018. Quantification of the seasonal hillslope water storage that does not drive streamflow. Hydrological processes, 32(13), pp.1978-1992.

Dunn, K.J., Bergman, D.J. and LaTorraca, G.A. eds., 2002. Nuclear magnetic resonance: Petrophysical and logging applications. Elsevier.

Falzone, S. and Keating, K., 2016. A laboratory study to determine the effect of pore size, surface relaxivity, and saturation on NMR T2 relaxation measurements. Near Surface Geophysics, 14(1), pp.57-69.

Falzone, S. and Keating, K., 2016. The NMR relaxation response of unconsolidated sediments during drainage and imbibition. Vadose Zone Journal, 15(6).

Faybishenko, B., Doughty, C., Steiger, M., Long, J.C., Wood, T.R., Jacobsen, J.S., Lore, J. and Zawislanski, P.T., 2000. Conceptual model of the geometry and physics of water flow in a fractured basalt vadose zone. Water resources research, 36(12), pp.3499-3520.

Flinchum, B.A., Holbrook, W.S., Grana, D., Parsekian, A.D., Carr, B.J., Hayes, J.L. and Jiao, J., 2018. Estimating the water holding capacity of the critical zone using near-surface geophysics. Hydrological Processes, 32(22), pp.3308-3326.

Flinchum, B.A., Holbrook, W.S., Parsekian, A.D. and Carr, B.J., 2019. Characterizing the critical zone using borehole and surface nuclear magnetic resonance. Vadose Zone Journal, 18(1), pp.1-18.

Foley, I., Farooqui, S.A. and Kleinberg, R.L., 1996. Effect of paramagnetic ions on NMR relaxation of fluids at solid surfaces. Journal of Magnetic Resonance, Series A, 123(1), pp.95-104.

Graham, R.C., Rossi, A.M. and Hubbert, K.R., 2010. Rock to regolith conversion: Producing hospitable substrates for terrestrial ecosystems. GSA today, 20(2), pp.4-9.

Grant, G.E. and Dietrich, W.E., 2017. The frontier beneath our feet. Water Resources Research, 53(4), pp.2605-2609.

Gu, X., Rempe, D.M., Dietrich, W.E., West, A.J., Lin, T.C., Jin, L. and Brantley, S.L., 2020. Chemical reactions, porosity, and microfracturing in shale during weathering: The effect of erosion rate. Geochimica et Cosmochimica Acta, 269, pp.63-100.

Gwo, J.P., Jardine, P.M. and Sanford, W., 2005. Effect of advective mass transfer on field scale fluid and solute movement: Field and modeling studies at a waste disposal site in fractured rock at Oak Ridge National Laboratory, Tennessee, USA. Hydrogeology journal, 13(4), pp.565-583.

Hahm, W.J., Rempe, D.M., Dralle, D.N., Dawson, T.E., Lovill, S.M., Bryk, A.B., Bish, D.L., Schieber, J. and Dietrich, W.E., 2019a. Lithologically controlled subsurface critical zone thickness and water storage capacity determine regional plant community composition. *Water Resources Research*, *55*(4), pp.3028-3055.

Hahm, W.J., Dralle, D.N., Rempe, D.M., Bryk, A.B., Thompson, S.E., Dawson, T.E. and Dietrich, W.E., 2019b. Low subsurface water storage capacity relative to annual rainfall decouples Mediterranean plant productivity and water use from rainfall variability. Geophysical Research Letters, 46(12), pp.6544-6553.

Hahm, W.J., Dralle, D.N., Sanders, M., Bryk, A.B., Fauria, K.E., Huang, M.H., Hudson-Rasmussen, B., Nelson, M.D., Pedrazas, M.A., Schmidt, L. and Whiting, J., 2022. Bedrock vadose zone storage dynamics under extreme drought: consequences for plant water availability, recharge, and runoff. Water Resources Research, p.e2021WR031781.

Hahm, W.J., Dietrich, W.E. and Dawson, T.E., 2018. Controls on the distribution and resilience of Quercus garryana: ecophysiological evidence of oak's water-limitation tolerance. Ecosphere, 9(5), p.e02218.

Hahm, W.J., Rempe, D.M., Dralle, D.N., Dawson, T.E., Lovill, S.M., Bryk, A.B., Bish, D.L., Schieber, J. and Dietrich, W.E., 2019. Lithologically controlled subsurface critical zone thickness and water storage capacity determine regional plant community composition. Water Resources Research, 55(4), pp.3028-3055.

Hahm, W.J., Rempe, D.M., Dralle, D.N., Dawson, T.E. and Dietrich, W.E., 2020. Oak transpiration drawn from the weathered bedrock vadose zone in the summer dry season. Water Resources Research, 56(11), p. e2020WR027419.

Hiller, T. and Klitzsch, N., 2018. Joint inversion of nuclear magnetic resonance data from partially saturated rocks using a triangular pore model. Geophysics, 83(4), pp.JM15-JM28.

Ireson, A.M., Mathias, S.A., Wheater, H.S., Butler, A.P. and Finch, J., 2009. A model for flow in the chalk unsaturated zone incorporating progressive weathering. Journal of Hydrology, 365(3-4), pp.244-260.

Kass, M.A., Irons, T.P., Minsley, B.J., Pastick, N.J., Brown, D. and Wylie, B.K., 2017. In situ nuclear magnetic resonance response of permafrost and active layer soil in boreal and tundra ecosystems. The Cryosphere, 11(6), pp.2943-2955.

Keating, K. and Knight, R., 2007. A laboratory study to determine the effect of iron oxides on proton NMR measurements. Geophysics, 72(1), pp.E27-E32.

Keating, K. and Knight, R., 2008. A laboratory study of the effect of magnetite on NMR relaxation rates. Journal of Applied Geophysics, 66(3-4), pp.188-196.

Keating, K. and Knight, R., 2010. A laboratory study of the effect of Fe (II)-bearing minerals on nuclear magnetic resonance (NMR) relaxation measurements. Geophysics, 75(3), pp.F71-F82.

Kirkland, C.M., Hiebert, R., Phillips, A., Grunewald, E., Walsh, D.O., Seymour, J.D. and Codd, S.L., 2015. Biofilm detection in a model well-bore environment using low-field NMR. Groundwater Monitoring & Remediation, 35(4), pp.36-44.

Klos, P.Z., Goulden, M.L., Riebe, C.S., Tague, C.L., O'Geen, A.T., Flinchum, B.A., Safeeq, M., Conklin, M.H., Hart, S.C., Berhe, A.A. and Hartsough, P.C., 2018. Subsurface plant-accessible water in mountain ecosystems with a Mediterranean climate. Wiley Interdisciplinary Reviews: Water, 5(3), p.e1277.

Lesparre, N., Girard, J.F., Jeannot, B., Weill, S., Dumont, M., Boucher, M., Viville, D., Pierret, M.C., Legchenko, A. and Delay, F., 2020. Magnetic resonance sounding measurements as posterior information to condition hydrological model parameters: Application to a hard-rock headwater catchment. Journal of Hydrology, 587, p.124941.

McCormick, E.L., Dralle, D.N., Hahm, W.J., Tune, A.K., Schmidt, L.M., Chadwick, K.D. and Rempe, D.M., 2021. Widespread woody plant use of water stored in bedrock. Nature, 597(7875), pp.225-229.

Mohnke, O., Jorand, R., Nordlund, C. and Klitzsch, N., 2015. Understanding NMR relaxometry of partially water-saturated rocks. Hydrology and Earth System Sciences, 19(6), pp.2763-2773.

Pedrazas, M.A., Hahm, W.J., Huang, M.H., Dralle, D., Nelson, M.D., Breunig, R.E., Fauria, K.E., Bryk, A.B., Dietrich, W.E. and Rempe, D.M., 2021. The relationship between topography, bedrock weathering, and water storage across a sequence of ridges and valleys. Journal of Geophysical Research: Earth Surface, 126(4), p.e2020JF005848.

Rempe, D.M., 2016. Controls on critical zone thickness and hydrologic dynamics at the hillslope scale. University of California, Berkeley.

Rempe, D.M. and Dietrich, W.E., 2018. Direct observations of rock moisture, a hidden component of the hydrologic cycle. Proceedings of the National Academy of Sciences, 115(11), pp.2664-2669.

Riebe, C.S., Hahm, W.J. and Brantley, S.L., 2017. Controls on deep critical zone architecture: A historical review and four testable hypotheses. Earth Surface Processes and Landforms, 42(1), pp.128-156.

Roth, K., Schulin, R., Flühler, H. and Attinger, W., 1990. Calibration of time domain reflectometry for water content measurement using a composite dielectric approach. Water resources research, 26(10), pp.2267-2273.

Rylander, E., Philip, M.S., Jiang, T. and Lewis, R., 2013, April. NMR T2 distributions in the Eagle Ford shale: reflections on pore size. In SPE Unconventional Resources Conference-USA. OnePetro.

Saidian, M. and Prasad, M., 2015. Effect of mineralogy on nuclear magnetic resonance surface relaxivity: A case study of Middle Bakken and Three Forks formations. Fuel, 161, pp.197-206.

Salve, R., Rempe, D.M. and Dietrich, W.E., 2012. Rain, rock moisture dynamics, and the rapid response of perched groundwater in weathered, fractured argillite underlying a steep hillslope. Water Resources Research, 48(11).

Schmidt, L. and Rempe, D., 2020. Quantifying dynamic water storage in unsaturated bedrock with borehole nuclear magnetic resonance. Geophysical Research Letters, 47(22), p.e2020GL089600.

Schwinning, S., 2010. The ecohydrology of roots in rocks. Ecohydrology: Ecosystems, land and water process interactions, Ecohydrogeomorphology, 3(2), pp.238-245.

Seyfried, M.S., Murdock, M.D., Hanson, C.L., Flerchinger, G.N. and Van Vactor, S., 2001. Long-term soil water content database, Reynolds Creek Experimental Watershed, Idaho, United States. Water Resources Research, 37(11), pp.2847-2851.

Walsh, D., Turner, P., Grunewald, E., Zhang, H., Butler Jr, J.J., Reboulet, E., Knobbe, S., Christy, T., Lane Jr, J.W., Johnson, C.D. and Munday, T., 2013. A small-diameter NMR logging tool for groundwater investigations. Groundwater, 51(6), pp.914-926.

Wan, J., Tokunaga, T.K., Williams, K.H., Dong, W., Brown, W., Henderson, A.N., Newman, A.W. and Hubbard, S.S., 2019. Predicting sedimentary bedrock subsurface weathering fronts and weathering rates. Scientific reports, 9(1), pp.1-10.

Ward, A.L., Caldwell, T.G. and Gee, G.W., 2000. Vadose zone transport field study: Soil water content distributions by neutron moderation (No. PNNL-13795). Pacific Northwest National Lab.(PNNL), Richland, WA (United States).

Ward, A.L. and Wittman, R.S., 2009. Calibration of a neutron hydroprobe for moisture measurements in small-diameter steel-cased boreholes (No. PNNL-18539). Pacific Northwest National Lab. (PNNL), Richland, WA (United States).